Protection of buried rigid pipes using geogrid-reinforced soil systems subjected to cyclic loading

Ahmed Elshesheny PhD research student, civil engineering department, faculty of engineering and informatics

University of Bradford, Bradford, West Yorkshire, BD7 1DP, UK.
Elshesheny.a@gmail.com

Mostafa Mohamed senior lecturer, civil engineering department, faculty of engineering and informatics

University of Bradford, Bradford, West Yorkshire, BD7 1DP, UK.
M.h.a.mohamed@bradford.ac.uk

Therese Sheehan lecturer, civil engineering department, faculty of engineering and informatics

University of Bradford, Bradford, West Yorkshire, BD7 1DP, UK.
T.Sheehan@bradford.ac.uk

Corresponding author:

Dr Mostafa Mohamed

Email: M.h.a.mohamed@bradford.ac.uk

Phone: +44(0) 1274 233856

Fax: +44(0) 1274 2341111

Resubmission

May 2020

Protection of buried rigid pipes using geogrid-reinforced soil systems subjected to cyclic loading

Ahmed Elshesheny, Mostafa Mohamed and Therese Sheehan

ABSTRACT: The performance of buried rigid pipes underneath geogrid-reinforced soil while applying incrementally increased cyclic loading was assessed using a fully instrumented laboratory rig. The influence of varying two parameters of practical importance was investigated; the pipe burial depth and the number of geogrid-layers. Measurements were taken for pipe deformation, footing settlement, strain in pipe and reinforcing layers, and pressure/soil stress on the pipe crown during various stages of cyclic loading. The research outcomes demonstrated a rapid increase in the rate of deformation of the pipe and the footing, and the rate of generated strain in the pipe and the geogrid-layers during the first 300 cycles. While applying further cycles, those rates were significantly decreased. Increasing the pipe burial depth and number of geogrid-layers resulted in reductions in the footing and the pipe deformations, the pressure on pipe crown, and the pipe strains. Redistribution of stresses, due to the inclusion of reinforcing layers, formed a confined zone surrounding the pipe providing it with additional lateral support. The pipe invert experienced a rebound, which was found to be dependent on pressure around the pipe and the degree of densification of the bedding layer. Data for strains measured in the geogrid-layers showed that despite the applied loading value and the pipe burial depth, the tensile strain in the lower geogrid-layer was usually higher than that measured in the upper layer.

Keywords: Geosynthetics, Buried rigid pipe, Incrementally cyclic loading, Pipe invert rebound, Passive arching, Slack effect.

1 ABBREVIATIONS

ITM	Induced trench method
EPS	Expanded Polystyrene
TDA	Tire-derived Aggregate
LVDT	Linear variable differential transducer
B	Footing width
L	Length of the reinforcing layer
u	Distance between the base of the footing and the upper reinforcing layer
h	Distance between two consecutive layers
H	Distance between the crown of the pipe and the ground surface
D	Outer diameter of the pipe
S	Settlement
F_S	Settlement of the footing
C_S	Settlement of the crown
I_S	Settlement of the invert
B_L	Bedding layer
LP	Loading phase
UL	Upper layer
LL	Lower layer
N	Number of the geogrid-layers

2 INTRODUCTION

The worldwide construction industry is increasing to an enormous extent to meet the needs and expectations of growing populations. This requires the construction of new houses, buildings, infrastructure and transportation links as well as providing sustainable solutions to protect and reduce potential risks on existing buried structures due to additional loads and stresses. Several research studies investigated the performance of buried flexible pipes under reinforced and unreinforced covers [1-11], however less attention has been given to buried rigid pipes. For decades, buried rigid pipes were widely used for several purposes, e.g. mineral transfer, due to their high circumferential and flexural stiffness. Nevertheless, additional static and dynamic loads would generate extra tensile stresses on the pipe wall, which will form cracks once exceeding the tensile strength of the rigid pipe material. It is therefore crucial that solutions are proposed and tested to provide protection by reducing the stresses on the buried rigid pipes.

Buried rigid pipes and structures behaviour was investigated using field tests and full-scale tests [12-19], numerical modelling [20-27] and large-scale experimental tests [22, 28, 29]. However, most of these studies were performed under static loading and during the installation process. Anderson [30] and Spangler [31] own the original work, which focused on the calculation of the diametric change of the pipe due to static loads. Strains in the walls of rigid pipes while laterally supporting them were investigated by [12, 19, 21]. It was reported that providing more lateral support kept the pipe safe, where tensile stresses were bearable. The relation between strains in the walls of buried pipes and the deformations that occurred in

these pipes was studied by Rogers, Fleming [32], where it was noted that the pipe deformation could be predicted using the measured strains. The influence of bedding layer thickness and density on the pipe behaviour was investigated by Abolmaali and Kararam [20] and Lay and Brachman [16]. It was reported that a thicker and lower density bedding layer could keep the pipe in safe condition, where reaction forces between the pipe and bedding layer were kept at minimum values. Large-scale experimental tests on concrete pipes subjected to seismic loading were investigated by Kim, Lynch [29]. Visual inspection illustrated the occurrence of considerable damage due to crack formation, as forces and bending moment severely influenced the pipe. Based on the aforementioned studies, it was concluded that tensile failure represented by the formation of cracks along the walls of the pipe occurred due to the stresses, strains and bending moments along its walls, where applied loads were transferred directly to it. In addition, static loading was applied in the aforementioned research studies, which does not represent the actual applied loads on many buried conduits in the real environment.

To reduce the tensile stresses and strains along the pipe walls, the Induced Trench Method (ITM) was introduced. Initial studies using ITM were conducted by [30, 33, 34]. ITM was reintroduced by Spangler [35] as Marston and Spangler (M-S) theory. The theory was about using compacted backfill over the buried pipe and the surrounding soils, then a trench of the same width as the pipe was excavated, where a thin compacted backfill layer remained above the pipe. The trench was then filled with loose lightweight material, which had high compressibility, leading

to the formation of active arching. At that time, a full description of the properties of the lightweight material was not available; consequently, ITM long-term behaviour was debated. A long time ago, leaves, straw, sawdust and woodchips were mixed with soil and used as lightweight backfill over the pipe [36-38]. The problem of these materials was their decomposition with the passage of time. Several research studies experimentally investigated the performance of superlight Expanded Polystyrene Blocks (EPS) as compressible material over different buried conduits to ensure the occurrence of active arching within the soil cover so as to reduce significantly the pressure on buried conduits where the lateral support was increased [13, 28, 39-41]. In addition, these values did not change over 3-years. Bartlett and Lingwall [42] investigated the influence of using EPS geofoam to enhance the seismic resilience of buried conduits, as well as protecting them from the detrimental effects of the permanent ground deformation, e.g. tectonic faulting and uplifting. It was reported that the inclusion of the EPS geofoam significantly decreased the vertical uplift forces and stresses affecting the buried conduits. Meguid and Youssef [43] investigated the contribution of tire-derived aggregate (TDA) layers above buried rigid pipes, instead of the superlight expanded polystyrene blocks. It was reported that measurements of the average pressure on top of the pipe were reduced by 30% compared with using granular backfill material above the pipe. TDA was an accepted replacement of superlight expanded polystyrene blocks in the ITM. Bartlett, Lingwall [44] and Witthoeft and Kim [45] performed numerical investigations on the influence of using compressible EPS geofoam to decrease earth pressure on buried pipes. It was

reported that the behaviour of the entire system depended on the properties of the EPS geofoam, where using EPS geofoam of lower density results in an enhanced performance of the system, which leads to reduction in the pressure on the buried conduits. In addition, EPS geofoam inclusion significantly contributed to decreasing the potential damage, which would affect buried conduits due to permanent ground deformations.

Since the main concept of the ITM and other earlier techniques to create lightweight backfill was to maintain buried conduit stability by reducing stresses on it, the inclusion of geogrid reinforcing layers instead of compressible material was adopted in this research as an alternative and sustainable approach. Geosynthetics were used for decades as soil reinforcing layers. The inclusion of these layers in the soil generates a new composite material of enhanced properties and performance, compared with natural soil. The interaction between the soil and the reinforcing layers, while applying static loading was investigated by [46-53]. On the other hand, the performance of reinforced soils while applying cyclic loading was performed by [54-57]. Data showed that the inclusion of reinforcing layers in the investigated systems significantly contributed to enhancing the bearing capacity of these systems. This was related to the load transfer mechanisms that formed between the reinforcing layers and soil particles, which depended on the geometry of the reinforcing layer and the size of the soil particles. Moreover, [58-60] investigated the protection concept of buried flexible pipes and existing voids using reinforcing layers, while applying repeated loading. It was noted that the inclusion of reinforcing layers provided protection to these

buried conduits through the stress distribution process and the lateral support that was provided. It should be noted that El Naggar, Turan [61] investigated experimentally and numerically the use of a bridging layer, which was formed by the inclusion of geogrid layers in granular fill, to reduce the pressure on buried utilities and to enhance the performance of embankments, under the application of static loading represented by the embankment's own-weight. It was reported that the bridging layer distributed the pressure and provided more protection to the buried conduit. Ahmed, Tran [62] performed experimental and numerical investigations on buried rigid pipes in geogrid-reinforced soil to measure the distribution of earth pressure on the pipe, and to study the soil-geogrid interaction. The contribution of the geogrid layer in reducing the pressure on the pipe was found to increase with the increase in the surface loading. It should be noted that a thick-walled PVC pipe was used to represent the buried rigid pipe, while applying surface loading. Moreover, the effect of varying the number of the reinforcing layers was not investigated.

According to the aforementioned literature, the use of geogrid reinforcement to enhance the behaviour of buried rigid pipes while applying incrementally increasing cyclic loadings has not been examined systematically under controlled conditions. In this study, the performance of buried rigid pipes underneath geogrid-reinforced soil while applying incrementally increased cyclic loading was investigated using a fully instrumented laboratory rig. In particular, two parameters of practical importance namely; the pipe burial depth and the number of geogrid-layers, were investigated. High quality data were generated for the footing

settlement, pipe deformation, strain in both the pipe and the reinforcing layers, and pressure on the crown of the pipe. To aid the discussion, the research outcomes are compared with results from controlled tests on the behaviour of buried concrete pipes in unreinforced sand beds by the authors [63].

3 TESTING RIG

To enable the experimental investigation for buried rigid pipes under geogrid-reinforced soil, a fully instrumented testing rig was designed and manufactured. It consisted of three parts: loading system, testing tank and data acquisition system, as shown in Fig. 1-A.

3.1 Loading system

A rigid loading frame was used to hold an Advanced Servo Hydraulic Actuator, forming the loading system. The capacity of the actuator was 1000 kN. The applied load was recorded using a load cell, which was installed in-between the loading area and the actuator. The loading profile amplitude was controlled using a computer program, which controlled the actuator. A loading profile, which was formed out of a monotonic loading phase followed by incrementally increased cyclic loading phases, was applied in this research to the investigated systems.

3.2 Testing tank

The detrimental effect of the boundary conditions, i.e. reaction interference, was avoided by designing the tank to be 1500 mm long, which is more than six-times both the diameter of the pipe and the width of the footing, as mentioned in previous studies [64-67]. Since the longitudinal direction of the pipe is much bigger than the other two dimensions, the model can be treated as a plane strain one.

Satu Niemi
Formatted
CS

Satu Niemi
Formatted
CS, Not Ita
grammar

Satu Niemi
Deleted:

Consequently, the strain in the longitudinal direction, i.e. length of the pipe, would tend to be zero, [60]. As a result, choosing the width of the tank to be 1000 mm is not expected to cause problems. The depth of the tank was chosen to be 1000 mm to allow installation of the pipe at three different burial depths. Consequently, a rigid testing tank, 1500 mm in length, 1000 mm in width, and 1000 mm in height was designed and manufactured, as schematically presented in Fig. 1-C. Rigid steel stiffeners and I-beams were used to maintain the rigidity of the walls and the base of the tank, respectively. The loading profile was applied to the investigated systems through a rigid steel strip footing, which was 990 mm in length and 200 mm in width. In real life, the pavement layer could behave as flexible or rigid depending on its structural performance. Flexible pavement relies on the shear strength of base and sub-base layers to transfer the stresses to a wider area resulting in a uniform pressure on the subgrade soil. Often flexible pavement suffers unequal deformation due to applied loading. On the other hand, rigid pavement incorporates the use of a concrete layer which would lead to the occurrence of uniform deformation as the rigid pavement will deform as a rigid body. Simulating a flexible asphaltic pavement is practically difficult in the laboratory, whereas a rigid pavement can be represented by a rigid footing. The measurement of the rigid footing deformation is also feasible in a controlled laboratory conditions. Similar experimental studies in previous researches were carried out using rigid loading plate, [59, 60]. The detrimental frictional effect between the footing and the walls of the tank was avoided by reducing the length of the footing by 10 mm compared with the width of the tank. Moreover, the footing

Satu Niemi
Formatted
CS

Satu Niemi
Formatted
CS, Not Ita
grammar

Satu Niemi
Deleted:

was placed in the centre of the tank to avoid any load eccentricity. The footing base was roughened using a heavy-duty sand paper to enable reflecting the applied pressure by traffic loading. Measuring the footing settlement was allowed using two Linear Variable Differential Transducers (*LVDTs*) considering the average value of them. The deformation of the invert of the pipe was measured using one LVDT installed underneath the pipe through a 20 mm hole, which was formed in the base of the tank. A rectangular section of the wall of the tank was replaced by a 25 mm thick transparent Perspex screen as demonstrated in Fig. 1-B, in order to visually inspect the pipe. A mechanism was developed using a rigid rod, nail and two LVDTs to measure the deformation of the crown of the pipe, as shown in Fig. 1-C. This mechanism was successfully used by the authors of a previous research paper, Elshesheny, Mohamed [2]. A smooth Polyethylene sheet covered the inner walls of the tank to minimize wall friction.

To measure the strain generated due to loading, strain gauges were fixed perpendicular to the longitudinal pipe direction on the inner crown, inner invert and the outer spring-line, where one strain gauge was used at each position. In addition, one strain gauge was installed at the middle longitudinal rib of each reinforcing layer to measure its strain, where it was parallel to the length of the layer (machine direction). The data logger was connected to the strain gauges by a half bridge circuit arrangement. Strain gauges could measure strains up to 5% and 2% for the reinforcement and the pipe, respectively. The pipe crown pressure was measured by installing an earth pressure cell 20 mm above the pipe crown, as presented in Fig. 1-C. After the testing process, the soil was removed carefully

Satu Niemi: Formatted CS
Satu Niemi: Deleted:
Satu Niemi: Formatted CS, Not Ita
Satu Niemi: Formatted CS
Satu Niemi: Formatted CS, Not Ita grammar
Satu Niemi: Deleted:
Satu Niemi: Formatted CS, Not Ita
Satu Niemi: Deleted:
Satu Niemi: Formatted CS

in order to scan and record the deformation of the reinforcement mid-point. Unfortunately, measurement of the vertical deformation of the reinforcement layer was not captured.

3.3 Data acquisition system

Measuring and recording the crown pressure, pipe and reinforcing layer strain, pipe deformation and footing settlement was facilitated using two data acquisition systems. Data were measured and recorded every 500 ms, according to the minimum allowed time interval of the data acquisition systems. All the measurement devices were calibrated before use to ensure the generation of high-quality data. All of the used instruments were calibrated, where the accuracy range of LVDTs varied between 0.03% and 0.81%. In addition, pressure and load cells achieved accuracies of 0.07% and 0.3%, respectively.

4 MATERIALS

4.1 Sand

Preparation of homogeneous testing beds, i.e. bedding layer and backfill cover, was performed using a relatively uniformly graded silica sand. Based on the specifications of the British Standard, BS 1377-1:2016, the sand was classified as Even-Graded, [68]. The experimentally acquired sand properties are presented in Table 1. Three triaxial tests were performed while varying the cell pressure to determine the stiffness of the sand considering the slope of the initial linear part of the stress-strain relationships. The average values of the initial tangent modulus and secant modulus from zero deviator stress to a deviator stress of 50 % of the peak deviator stress which is a commonly used value to examine foundation

Satu Niemi
Formatted
and gramm
Satu Niemi
Deleted:

problems [69], were determined and found to be 55 MPa and 54 MPa respectively. These results confirmed the linearity of the initial stress-strain relationships attained for the used sand. Preparation of homogeneous sand beds was achieved by using a raining technique, where sand was poured through a perforated screen with 5 mm holes from a 500 mm dropping height. The dry unit-weight of the sand was measured at different locations in the tank to ensure preparing homogeneous sand beds. The dry unit-weight of the sand was found to be 16.32 ± 0.02 kN/m^3, which would ensure the consistency of the prepared sand beds. The dry unit-weight of the sand beds were found to be 99% of the maximum dry unit-weight obtained according to the standard Proctor test.

4.2 Rigid pipe

A flexible pipe has the ability to endure vertical diametric strain of at least 2% without the occurrence of any structural instability, unlike the rigid one [71]. In this research, a 230 mm outer diameter concrete pipe, which has a length and wall thickness of 990 mm and 14 mm, respectively, was utilized. A predesigned casting mold, which was successfully used by the authors [63], was used to prepare rigid concrete pipes in the laboratory. To eliminate any friction between the pipe and the walls of the tank, the pipe was shortened 10 mm, where foam strips were used to seal the clearance formed as shown in Fig. 1-B. The determination process of the compressive strength of the pipe material, i.e. concrete, was facilitated using cubic concrete specimens with a side length of 100 mm. Based on the British Standard specifications, BS EN 12390-3:2009 [72], the cubes were tested under compressive loading after 28-days. According to the maximum sustained load by

Satu Niemi
Formatted
CS

Satu Niemi
Formatted
CS, Not Ita
grammar

Satu Niemi
Deleted:

each specimen, the average compressive strength of the concrete was found to be 68 MPa. Results showed that the unit weight and the elastic modulus of the pipe material were 23 kN/m^3 and 35000 MPa, respectively.

4.3 Geogrid reinforcement

The reinforced sand beds were prepared using biaxial geogrid reinforcement, SS20. Table 2 illustrates the experimentally acquired mechanical properties of the reinforcing layers, according to the specifications of the British Standard, BS EN ISO 10319:2015, which indicated that at least five specimens of 200 mm in width should be tested under the application of a uniform tensile force, [73]. Measurements of stress-strain behaviour of the reinforcing layers indicated that the elastic modulus of the material is 300 MPa.

Satu Niemi
Formatted
and gramm
Satu Niemi
Deleted:

5 CYCLIC LOADING

The National Annex of the British Standard, NA to BS EN 1991-2:2003, demonstrates that traffic loads are one of the major factors that severely affect buried pipes. The load applied to the buried pipe results from the wheel load, which depends on the overall load of the vehicle, number of axles and number of wheels per axle, [74]. In general, the average value of an axle load would range between 50 and 230 kN, which can generate a wide range of pressure on the ground surface and buried pipes. According to the axle load and the square contact area between the ground surface and the wheel, which has a side of length 350 mm, a range of average pressure from 200 to 950 kPa would be generated. In this research the existence of a pavement layer above the soil surface was not considered and consequently reducing the applied surface

pressure value would be feasible, as formerly suggested and executed by Mehrjardi and Tafreshi [75] and Tafreshi and Khalaj [60]. In this investigation, the applied loading profile consisted of two stages, monotonic and cyclic, as illustrated in Fig. 2, Table 3 demonstrates the cyclic loading values during the different phases of the applied loading profile. Since the load was applied using a hydraulic actuator, a monotonic loading had to be applied before the repeated loading to maintain pressure value between the actuator and the footing. If the pressure value between the actuator and the footing reached zero, it may not have been possible to maintain control over the actuator. This is why it is important to apply monotonic loading step before applying the repeated loading. Of note, a monotonic loading was applied to the pipe-soil systems investigated in this research until the mean cyclic loading value was reached. This stage was followed by the application of a number of cyclic loading phases, which varied according to each test. At the beginning of the research, a soil-pipe system was tested while applying a static load in order to attain a realistic monotonic load value. Based on the results of the static loading test (data are not presented), 13 kN and 5 kN were selected as values of the monotonic load and load amplitude in subsequent cyclic loading phases, respectively. It should be noted that the implementation of the first cyclic loading phase required the application of 3000 cycles to reach stagnation in the system response. However, the subsequent cyclic loading phases were performed for only 1000 cycles each, which were enough to present the response of the system. The adopted number of cycles in the first and the subsequent loading phases was similar to that used by the authors in previous research

Satu Niemi
Formatted
CS

Satu Niemi
Formatted
CS, Not Ita
grammar

Satu Niemi
Deleted:

Satu Niemi
Formatted
and gramm

Satu Niemi
Deleted:

357 papers [63]. The number of applied cyclic loading phases varied according to each
358 test, where no additional loading phases were applied when the pipe was
359 obviously cracked or the footing was excessively settled, which represented
360 system failure. The loading profile represented different vehicle capacities or load
361 increase with the passage of time. The utilized data acquisition systems could take
362 measurements every 500 ms, as a minimum interval of time, and consequently,
363 the frequency of the cyclic loading was selected to be 0.5 Hz, so that four readings
364 could be measured in every single cycle.

365 ## 6 TESTING PROGRAMME

366 The testing programme followed in this research is presented in Table 4. Fig. 1-C
367 shows a schematic diagram of the parameters to be tested. The influence of
368 varying two parameters was investigated in this research, the number of geogrid-
369 reinforcing layers and the pipe burial depth relative to its diameter (*H/D*). In total,
370 seven tests were undertaken. It is worth noting that optimum values of both,
371 spacing between the geogrid-layers (h/B), and spacing between top most layer
372 and the footing (u/B) were chosen based on recommendations of previous
373 researches, [60, 75, 76]. Earlier study [20] demonstrated significant effects for the
374 packing condition of the bedding soil and bedding thickness on stress reduction in
375 the buried pipe wall. In addition, it was found that the packing condition of the
376 bedding soil is more dominant over the bedding thickness which was studied up to
377 0.37 of the pipe diameter. In this study, the bedding soil was compacted to 99 % of
378 the maximum dry unit weight achieved by the Standard Proctor Test which would
379 diminish the effect of bedding thickness. Consequently, a bedding thickness of 150

Satu Niemi
Deleted:
Satu Niemi
Formatted
CS, Not Ita
grammar
Satu Niemi
Deleted:
Satu Niemi
Formatted
and gramm
Satu Niemi
Formatted
CS

mm which is 0.65 of the pipe diameter was selected and kept constant in all tests to ensure an adequate interaction between the buried pipe and bedding soil.

7 REPEATABILITY

In Series D, test 10 was executed to ensure the generation of accurate data of high-quality. This test was a repetition for test 4 (series B), with the same testing conditions. Careful inspection of the data illustrated that an excellent match was achieved between the two tests (data not presented). However, by reaching the pipe-soil systems failure, the footing settlements were varied slightly, where the maximum observed variation value was 3%. Affirmation of the appropriate preparation of the investigated pipe-soil systems and the reliability of the tests was confirmed by the excellent match achieved between the outcomes of the two tests.

8 RESULTS AND DISCUSSIONS

The effects of changing both the pipe burial depth and the number of reinforcement layers on the overall performance of the reinforced soil-pipe systems were evaluated and discussed. Pipe crown pressure, strains in both the reinforcement and the pipe, pipe deformations, and the footing settlement were carefully discussed. Deformations of both the footing and the pipe were presented as a normalized ratio with respect to the pipe diameter.

8.1 Unreinforced case, Series A

Series A of the testing program investigated the contribution of *H/D* variation to the performance of buried pipes in unreinforced sand. The tested pipe-soil systems sustained a maximum of five loading phases, as illustrated in Table 3, until failure

Satu Niemi
Formatted
and gramm

Satu Niemi
Deleted:

occurred. The description and results of the unreinforced case is presented in [63], where a comparison between some of the results and the outcomes of this research are presented.

8.2 Reinforced case

Two series (B and C) were conducted to investigate the influence of geogrid-reinforcement inclusion on load transfer and reinforced soil-pipe system load capacity. Table 3 illustrates the magnitude of the applied cyclic load in Series B and C, at different phases. The variation of both the number of reinforcing layers and the pipe burial depth is discussed in this section.

8.2.1 Settlement of the footing

The variation in the normalised footing settlement ratio (F_s/D) in relation to the number of loading cycles is demonstrated in Fig. 3. It was noted that the decrease in the footing settlement is dependent on the increase in both pipe burial depth and number of reinforcing layers. Moreover, the tested pipe-soil systems were allowed to endure more phases of cyclic loading until the occurrence of system failure.

It was observed that while applying the monotonic loading; the footing settlement in the three burial depths of each testing series were approximately equal. There was slight variation in the measured values of the normalised footing settlement, where the average values were 1.33%, 1.18% and 0.9% for Series A, B and C, respectively, with enhancement ratios of 11.3% in Series B and 32.3% in Series C, compared with Series A. While applying the 1st loading phase, an obvious variation was observed in the settlement of the footing, where the maximum settlement rate

Satu Niemi
Formatted
and gramm

Satu Niemi
Deleted:

Satu Niemi
Formatted
CS, Not Ita
grammar

Satu Niemi
Deleted:

Satu Niemi
Formatted
CS

was observed within the first 300 cycles of the first loading phase in each test. The maximum normalised settlement value occurred in *T1*, where its value was 2.74%, while the minimum value occurred in *T9* with a value of 1.6%. Significant decrease in the settlement rate occurred with the progression of loading cycles until reaching a stable rate at the end of the loading phase, where the normalised settlement values reached 4.7% and 2.3% for *T1* and *T9*, respectively. Under subsequent applied loading phases, the settlement of the footing underwent the same behaviour, where its settlement rate increased slightly at deep burial depths, i.e. *H/D*=2 and 2.5, and significantly at shallow burial depths, i.e. *H/D*=1.5, until failure occurred, which was represented by a sudden increase in the settlement rate of the footing.

Fig. 4 shows the relationship between the normalised footing settlements once reaching the end of the applied loading phases, and the increase in the pipe burial depth in Series C, where two reinforcing layers were utilised. A reduction in the settlement of the footing occurred while increasing the pipe burial depth during the application of any loading phase. For example, at the 9th loading phase, the normalised settlements of the footing were 7.26%, 5.83% and 5.43% at *H/D*=1.5, 2 and 2.5, respectively. The ratio of enhancement reached 19.7% and 25.2% at *H/D*=2 and 2.5, compared with the case of *H/D*=1.5. A slight reduction in the rate of settlement was noticed during the initial loading phases, where this rate was increased while applying advanced loading phases. Fig. 5 illustrates the relation between the normalised footing settlement and the progression of the cyclic loading phases to clarify the variation that occurred in the rate of settlement of the

Satu Niemi
Formatted
CS

Satu Niemi
Formatted
CS, Not Ita
grammar

Satu Niemi
Deleted:

Satu Niemi
Formatted
CS

Satu Niemi
Formatted
CS, Not Ita
grammar

Satu Niemi
Deleted:

456 footing. In *T7*, where *H/D*=1.5, the rate of settlement increased from the 1st to the
457 2nd loading phases by 9.8%, and this ratio was increased to 15% from the 8th to
458 the 9th phases. The system did not withstand any additional loading phases as
459 failure occurred because of the measured increase in the rate of settlement of the
460 footing. In *T8* and *T9*, similar behaviour of the footing settlement rate was
461 observed. Consequently, at the same burial depth, while applying the initial
462 loading phases, a slow increase in the rate of settlement of the footing occurred,
463 where this rate became noticeably higher with the progression of the loading
464 phases. This behaviour continued until failure occurred.
465 It was obvious that footing settlement decreased gradually with the inclusion of the
466 reinforcing layers, where a new composite system with enhanced properties was
467 formed, particularly the shearing resistance. It was noted that in Series B and C,
468 the number of the loading cycles endured by the tested pipe-soil systems was
469 much higher than those endured in Series A. This could be attributed to the
470 interaction that formed between the transverse ribs of the reinforcing layers and
471 the soil trapped inside its apertures, which is defined as the passive earth
472 resistance mechanism. This interaction allows the tensile stresses and strains to
473 be transferred from the soil to the reinforcing layers, leading to a significant
474 decrease in the lateral movement of the soil and increased confinement. This
475 behaviour enables soil in the region below footing to resist high shear stresses,
476 leading to a reduction in footing settlement. The number of loading phases
477 endured was the highest in Series C, which could be attributed to the inclusion of
478 two reinforcing layers resulting in an increase in the trapped soil volume in-

between the reinforcing layer apertures. It was noted that the settlement rate and value were the highest during the first 300 cycles of the first loading phase. This could be attributed to the slack effect, where the reinforcing layers were stretched due to the applied loads before they contributed to the pipe-soil system stability. The settlement rate rapidly increased once more at the loading phase, where failure occurred.

8.2.2 Pipe crown pressure

Fig. 6 illustrates the values of pipe crown pressure precisely at its mid-section due to burial depth increase in Series B, while using one layer of reinforcement. Increasing the burial depth of the pipe contributed significantly to reducing the pressure along its crown. Applying the monotonic loading generated pressure of 69 kPa, 53.5 kPa and 35.4 kPa in *T4*, *T5* and *T6*, respectively, on the crown of the pipe, whilst the footing pressure was 65 kPa. The pressure reduction ratio reached 22.5% and 48.7% for *T5* and *T6*, respectively, compared with that measured in *T4*. The pressure in *T4* was slightly higher than that applied on the footing by 5.8%. This could be attributed to i, self-weight of the soil above the pipe and ii, passive arching mechanism due to the difference in stiffness between the soil and the pipe, which attracted the pressure in the adjacent soil portions to the pipe. Visual observations at this stage illustrated no crack formation along the pipe, despite the increased pressure in *T4*. In the 1st cyclic loading phase, particularly after applying the first 300 cycles, the maximum pressure rate on the crown was observed, where the pressure values were 101 kPa, 73.2 kPa and 42.5 kPa for *T4*, *T5* and *T6*, respectively, however the applied pressure to the footing was 90 kPa. The

Satu Niemi
Formatted
CS

Satu Niemi
Formatted
CS, Not Ita
grammar

Satu Niemi
Deleted:

503 pressure value in *T4* was higher than that applied to the footing by 10.9%;
504 however, the pressure curve illustrated no crack formation, as the pressure value
505 and rate were stable without any variation. With further cycles of loading during the
506 1st loading phase, the pressure generation rate was significantly decreased, where
507 the pressure value remained almost constant until reaching the end of the 1st
508 loading phase. This was clear evidence that the pipe was still attracting pressure
509 without the formation of any cracks. The inclusion of the reinforcing layer
510 distributed the applied pressure along its plane, where a pressure of a lower value
511 was transferred underneath the reinforcing layer. Due to this pressure distribution,
512 additional pressure was applied to the soil regions surrounding the pipe, which
513 provided additional lateral support, and enhanced the confinement of the pipe,
514 which in turn allowed the pipe to sustain higher pressure without the formation of
515 cracks.
516 While applying further cyclic loading phases, an increase in the values of pressure
517 occurred until reaching the 5th loading phase in *T4* and the 6th loading phase in *T5*
518 and *T6*. In *T4*, and during the 5th loading phase, it was observed that the pressure
519 value and rate decreased slightly, however the pressure value at the end of the 5th
520 loading phase was 203 kPa, which is still higher than that applied to the footing by
521 6.4%. This illustrated the initiation of the passive arching mechanism collapse,
522 where cracks were visually observed at this stage. For *T5* and *T6*, a similar
523 collapse in the passive arching mechanism was observed during the 6th loading
524 phase, where the pressure transfer rate slightly decreased, and hairline cracks
525 were observed. After these loading phases, it was observed that the pressure rate

526 and value significantly decreased, which was a clear sign that the pipe could not
527 sustain any additional pressure, which could be attributed to the loss of its strength
528 due to the cracks that had formed.
529 In *T4*, and during the 6th loading phase, the pressure transfer rate decreased
530 significantly, to 220 kPa and 194 kPa at the 300th and the last cycles of the 6th
531 loading phase respectively. The pressure value at the end of the loading phase
532 was less than the applied pressure by 9.8%, which can be considered as evidence
533 of the collapsed passive arching mechanism and the initiation of active arching. In
534 *T5* and *T6*, the collapse that occurred in the passive arching became more
535 obvious because of loading phase progression, where the reduction rate of the
536 pressure transfer curves increased until the occurrence of system failure. Similar
537 behaviour was observed in Series C, where the tested systems sustained
538 additional loading phases due to the inclusion of two layers of reinforcement. It is
539 clear that the presented behaviour of the pressure along the crown matches with
540 the measured footing settlement, i.e. Fig. 3. The measured value of footing
541 settlement in T4 was the highest, consequently, higher value of pressure was
542 transferred to the pipe leading to quicker failure occurrence compared with T5 and
543 T6.
544 Generally, a differential settlement was formed between the soil column
545 underneath the footing and the adjacent soil regions due to the application of loads
546 on the footing, which generated shearing stresses between these regions of soil
547 as well as the formation of an arching effect [77]. Since the pipe was a rigid one,
548 its stiffness was significantly higher than the soil's, and consequently its ability to

Satu Niemi
Formatted
CS

Satu Niemi
Formatted
CS, Not Ita
grammar

Satu Niemi
Deleted:

attract load was increased, which generated a passive arching mechanism [13, 19, 78]. Pipe crown pressure was the summation of three mechanisms, passive arching, load mitigation and distributed load over the reinforcing layer. The distributed load over the reinforcing layer mechanism was generated due to the inclusion of the reinforcing layers. In this mechanism, the reinforcing layer and the trapped soil in-between its apertures formed a stiff composite layer, where the pressure was distributed along its plane generating a wider loaded area with a lower pressure value underneath it. This mechanism depended on the passive earth resistance between both the reinforcing layer and the soil. Increasing the number of the reinforcing layers increased the contribution of this mechanism. At shallow burial depths, the passive arching mechanism controlled the value of pressure on the pipe, where the lower soil layer was allowed to interact in the load mitigation mechanism, decreasing its contribution. Conversely, the contribution of the load mitigation mechanism dominated the system performance at deeper burial depths, where more layer of soil mitigated pressure above the pipe. This contributed to decreasing the pressure on the crown of the pipe, which agreed with the findings of [66]. The intensive inclination in the pressure curve is a clear sign that the tested pipe-soil systems were in the failure phase, where the increase in the tensile strain values contributed to the formation of cracks along the pipe leading to stress redistribution and system failure.

Fig. 7 presents recorded data for the pipe crown pressure due to the inclusion of the reinforcing layers at burial depth of *H/D*=1.5. Due to the application of the monotonic loading, the pressure above the crown reached 86 kPa, 69 kPa and 62

Satu Niemi
Formatted
CS

Satu Niemi
Formatted
CS, Not Ita
grammar

Satu Niemi
Deleted:

574 kPa for *T1*, *T4* and *T7* respectively, with reduction ratios of 19.8% for *T4* and
575 27.9% for *T7* relative to *T1*. With the application of the 1st cyclic loading phase, the
576 300th cycle pressure values were 106.8 kPa, 101 kPa and 96 kPa, respectively.
577 With the application of further cycles, it was observed that the pressure values in
578 *T4* and *T7* remained almost constant until reaching the end of the 1st loading
579 phase, which indicated that the pipe was able to attract loads without forming any
580 cracks. In *T1*, the unreinforced case, it was observed that the pressure value along
581 the crown followed a non-uniform behaviour, where the pressure value decreased
582 in between the 300th and the 600th cycles and then became almost constant until
583 reaching the 1500th cycle, then it decreased until reaching the end of the 1st
584 loading phase, with details provided in [63]. By visual inspection, the formation of
585 cracks in *T1* during the 1st loading phase were observed, which indicated that the
586 pipe could not attract load anymore and the controlling passive arching
587 mechanism started to collapse, where the pressure value was still higher than the
588 applied one.

589 Careful inspection of Fig. 7 indicated that the inclusion of reinforcing layers slightly
590 decreased the pressure on the pipe; however, it provided significant lateral support
591 to it, through the redistribution of stresses along the reinforcing layer plane, which
592 allowed for more loading phases to be sustained. In *T1*, pipe failure, i.e. crack
593 formation, was noticed during the 1st loading phase, where in *T4* and *T7* cracks
594 were formed in the 5th and 10th loading phases, respectively.

Satu Niemi
Formatted
CS

Satu Niemi
Formatted
CS, Not Ita
grammar

Satu Niemi
Deleted:

8.2.3 Crown settlement

Fig. 8 illustrates the values of the normalised crown settlements (C_s/D) due to varying the pipe burial depth, for Series B and C. It was clear that increasing the pipe burial depth while inserting the reinforcing layers into the tested pipe-soil systems had a significant effect on decreasing the crown settlement. Both, the number of reinforcing layers and the pipe burial depth governed the reduction rate in the crown settlement, which was similarly noted for the occurred decrease in the footing settlement presented in Fig. 3, and the pressure values recorded along the crown of the pipe as shown in Fig. 6 and Fig. 7.

It was clear that the maximum settlement rate of the crown occurred at the shallowest burial depths, e.g. in *T4* and *T7*, during the first 300 cycles of the 1st loading phase, where the normalised settlement values reached 0.67% and 0.57% respectively, which was lower than that measured in *T1* by 8.2% and 21.9%. With the advancement of loading cycles, the settlement rate decreased smoothly until reaching a steady rate in *T4* and *T7* by reaching the end of the 1st loading phase, where the normalised settlement values were 1.25% and 1.12%, respectively, with reduction ratios of 16.1% and 24.8% compared with *T1*. With the application of further loading phases, it was observed that the crown settlement increased within the 1st 300 cycles of every loading phase and then the rate was decreased with progressive cycles until reaching the end of the phase, where a slight increase in the settlement rate was observed at deeper burial depths, while at shallow burial depths the settlement rate was significant.

Satu Niemi: Formatted CS
Satu Niemi: Formatted CS, Not Ita grammar
Satu Niemi: Deleted:
Satu Niemi: Deleted:
Satu Niemi: Formatted CS
Satu Niemi: Formatted CS, Not Ita grammar
Satu Niemi: Formatted CS, Not Ita grammar
Satu Niemi: Deleted:
Satu Niemi: Deleted:
Satu Niemi: Formatted CS
Satu Niemi: Formatted CS
Satu Niemi: Formatted CS, Not Ita grammar

It was noted that the crown settlement rate at shallow burial depths was very rapid until reaching the 300th cycle of the 1st loading phase, where the reinforcing layers were in the stretching phase, known as the slack effect [79-82]. Once the slack effect ended, the reinforcing layers contribution in decreasing the crown settlement was initiated through the formation of the mechanisms of membrane effect and distributing load over the reinforcing layers. It was observed that the crown settlement rate decreased smoothly until reaching a steady rate forming a uniform settlement pattern. A non-uniform settlement pattern was observed in *T1*, where cracks were generated due to the lower lateral support, leading to stress fluctuations along the pipe with the application of loading cycles.

At deeper burial depths, it was observed that the maximum settlement rate occurred at a slightly lower number of cycles than that of the shallow burial depths, where the settlement value was significantly lower in the deep burial depths. Increasing the pipe burial depth contributed in providing more lateral support to it, due to the increased soil self-weight. In addition, the inclusion of reinforcing layers resulted in a pressure distribution over a wider area. This led to a pressurising process for the soil regions adjacent to the pipe, which increased the lateral support provided to the pipe contributing to the decrease of its crown settlement rate and value.

8.2.4 Invert settlement

Fig. 9 shows the normalised invert settlements values (I_S/D), while varying *H/D,* for Series C. It is clear that while applying loading phases, the pipe invert experienced downward settlement which was followed by upward one, representing a rebound

Satu Niemi
Formatted
CS

Satu Niemi
Formatted
CS, Not Ita
grammar

Satu Niemi
Deleted:

646 occurrence. Pipe burial depth, applied load, and number of reinforcing layers
647 governed the occurrence of this behaviour. At shallow burial depths, i.e. *T4* and
648 *T7*, the rebound occurred during the 1st loading phase once the normalised invert
649 settlement reached 0.39% and 0.32%, respectively, which was lower than that
650 measured in *T1* by 8.47% and 24.9%. The increase of the number of geogrid-
651 layers and the pipe burial depth hindered the occurrence of rebound due to
652 decreasing the pressure along the pipe and enhancing the confining effect
653 surrounding the pipe, as presented in Fig. 6 and Fig. 7.
654 In *T1*, the bedding layer was rapidly densified forming a stress concentration zone
655 along the invert, which led to the formation of a hair-crack. This behaviour initiated
656 a collapse in the passive arching mechanism, as shown in Fig. 7, decreasing the
657 pressure along the crown and increasing it around and underneath the pipe [63].
658 Consequently, a rebound in the invert deformation was initiated. In *T4* and *T7*, no
659 cracks were formed along the invert of the pipe during the 1st loading phase but
660 the rebound occurred. The concrete pipe behaved as a rigid support that attracted
661 the applied loads because of its high stiffness. Consequently, its invert behaved as
662 a support to the pipe itself, where its main function was to transfer load to the
663 bedding layer underneath it. Stiffness variation between the invert and the bedding
664 layer formed a stress concentration zone between them. With the progression of
665 the loading cycles, the density of the soil was increased, i.e. soil densification.
666 Consequently, increased stresses were generated between the bedding layer and
667 the invert, matching the findings of Abolmaali and Kararam [20]. Moreover, the
668 upward reaction forces between them increased as well, initiating the invert

Satu Niemi
Formatted
CS

Satu Niemi
Deleted:

Satu Niemi
Formatted
CS, Not Ita
grammar

Satu Niemi
Formatted
CS

Satu Niemi
Formatted
CS, Not Ita
grammar

Satu Niemi
Deleted:

Satu Niemi
Formatted
CS, Not Ita
grammar

Satu Niemi
Deleted:

Satu Niemi
Formatted
CS

rebound. In addition, the enhanced confinement effect of the soil regions surrounding the pipe due to the existence of the reinforcing layer provided more resistance to the pipe against deformation forcing its invert settlement to rebound under the applied upward stresses along its invert. Fig. 7 illustrated that the passive arching mechanism in *T7* did not collapse during the first loading phase, despite the invert rebound that occurred, as shown in Fig. 9. This illustrates that the invert rebound is not an indication for tensile failure, and the rebound is dependent on the test configuration.

At deeper burial depths, a smooth invert rebound occurred during further loading phases, at the 3rd and 4th loading phases for *T8* and *T9*, respectively. This can be attributed to the enhanced lateral support provided to the pipe because of the existence of the reinforcing layers, which led to redistribution of the pressure around the pipe allowing it to sustain further loading phases, as presented in Fig. 7. Consequently, the system required an increased number of loading cycles to increase the stiffness of the bedding layer, which would generate a feasible upward pressure along the invert of the pipe, initiating its rebound.

In the reinforced and unreinforced cases, the invert rebound was very sharp at a shallow burial depth and occurred during the 1st loading phase. While increasing the pipe burial depth, the rebound occurred gradually under applying further phases of the cyclic loading.

8.2.5 Pipe cross-section deformed shape

According to the findings of the invert and the crown settlements of the pipe, it was clear that under all loading phases the pipe crown settled downward, despite the

Satu Niemi
Formatted
CS

Satu Niemi
Deleted:

Satu Niemi
Formatted
CS, Not Ita
grammar

Satu Niemi
Formatted
CS

Satu Niemi
Formatted
CS, Not Ita
grammar

Satu Niemi
Deleted:

Satu Niemi
Formatted
CS

Satu Niemi
Formatted
CS, Not Ita
grammar

Satu Niemi
Deleted:

number of reinforcing layers and the pipe burial depth. On the other hand, the pipe invert experienced downward settlement followed by upward movement depending upon the amount of reinforcement, cyclic loading phase and pipe burial depth. These two opposite responses played a vital role in shaping the deformed pipe cross-section, which depended on the reduction in the vertical diameter and the increase in the horizontal one. The initial circular cross-section of the pipe was divided into four segments in between the cracks, and deformed to form an elliptical shape, as presented in Fig. 10. The inclusion of reinforcing layers and increasing the burial depth in the tested systems hindered and controlled the crack formation and propagation; moreover, they contributed to enhancing the systems performance and allowed them to sustain a greater number of loading phases, until failure occurred, as presented in the pressure curves, Fig. 7.

8.2.6 Pipe strain

Due to the pressure transferred from the soil to the pipe and because of the pipe-soil interaction, tensile and compressive strains were generated in the pipe. Strain gauges were fastened at three controlling locations, the inner crown, invert and outer spring-line, since the pipe experienced tensile strain along these lines. Once tensile strain value exceeds the tensile strength of the pipe, cracks formation is expected.

Invert strain

Pipe invert strain for the three tested series was illustrated in Fig. 11. An obvious reduction was observed in the strain rate and its value while increasing the burial depth of the pipe and the inclusion of reinforcing layers, which also controlled the

Satu Niemi: Formatted CS
Satu Niemi: Deleted:
Satu Niemi: Formatted CS, Not Ita grammar
Satu Niemi: Formatted CS
Satu Niemi: Formatted CS, Not Ita grammar
Satu Niemi: Deleted:
Satu Niemi: Formatted CS, Not Ita grammar
Satu Niemi: Deleted:
Satu Niemi: Formatted CS

behaviour of the invert settlement, Fig. 9. Strain generated along the invert of the pipe was a reflection to the soil stress transferred to the pipe presented in Fig. 7. At a shallow burial depth, for *T1*, *T4* and *T7*, it was observed that the strain generation rate while applying the monotonic loading was very rapid, as the pipe experienced high value of soil stress during short period of time, where the strain values were equal to 0.02%, 0.016% and 0.012%, respectively. While applying the 1st loading phase, the strain in *T1* followed a non-uniform pattern, which was related to the soil stress on the pipe and the early formation of cracks. In *T4* and *T7*, no cracks were formed during the 1st loading phase, and an average rapid strain rate of 85% was observed until reaching the 300th cycle, which was more rapid than that observed in *T1*. With further loading cycles until reaching the end of the 1st loading phase, the strain rates were decreased to 67.6% and 77.5% for *T4* and *T7*, respectively, where strain values were less than that measured in *T1* with 7.5% for *T4* and 20.2% for *T7*. This decrease in the strain rate could be attributed to the end of the reinforcing layers slack effect, i.e. the extension of the layer before the initiation of its contribution to the system stability. With the advancement of loading phases, the rate of strain increased during the 1st 300 cycles and then it decreased, where a stable rate controlled the strain pattern until reaching the end of the loading phase. Failure occurred when a rapid increase in the strain rate was observed, which was not followed by a decrease due to further loading cycles.

At deeper burial depths, *H/D*=2 and 2.5, a uniform strain pattern was observed, where strain rate increased within the 1st 300 cycles of every phase of loading, and

Satu Niemi
Formatted
CS

Satu Niemi
Formatted
CS, Not Ita
grammar

Satu Niemi
Deleted:

Satu Niemi
Formatted
CS

Satu Niemi
Formatted
CS, Not Ita
grammar

Satu Niemi
Deleted:

749 then it decreased to follow a more stable rate until reaching the final cycle of the
750 loading phase. Increasing the pipe burial depth and the inclusion of the reinforcing
751 layers decreased the strain along the invert. In *T9*, where two layers of
752 reinforcement were used, the strain value at the end of the 1st phase of loading
753 was 0.02%, where it was lower than that measured in *T6* (one layer) and *T3*
754 (unreinforced) by 4% and 55.5%, respectively. This illustrated that the contribution
755 of inserting a reinforcing layer is obvious at the initial loading phases; however, the
756 number of reinforcing layers insignificantly influenced the system behaviour, which
757 could be attributed to the relatively low value of the applied loads. At the 6th
758 loading phase, *T3* did not sustain the applied loads, and failure occurred. On the
759 other hand, the strain along the invert in *T9* was lower than that measured in *T6* by
760 18.5%. This illustrated that increasing the number of reinforcing layers increased
761 their contribution in enhancing the system performance with the progression of the
762 applied loading phases. At a relatively higher value of applied loads, the lower
763 reinforcing layer suffered more deformation relative to the 1st loading phase,
764 leading to enhancing the contribution of the membrane mechanism, which in turn
765 enhanced the behaviour of the reinforced soil above the pipe leading to a further
766 reduction in the strain in the pipe. In general, in the unreinforced series the pipe
767 experienced significantly larger strain values along its invert compared with the
768 reinforced series, where a low-confined soil zone surrounded the pipe and no
769 membrane mechanism enhanced the performance of the backfill cover because of
770 the absence of reinforcing layers. The reinforcing layers enabled the tested

771 systems to endure a greater number of loading phases safely, where the pipe
772 sustained lower strain values, particularly during the advanced loading phases.
773 To clearly illustrate the influence of inserting and increasing the number of the
774 geogrid-reinforcing layers on decreasing the strain generated along the invert of
775 the pipe, Fig. 12 was plotted. Fig. 12 presents a relation between the strain
776 generated along the invert of the pipe and the number of the geogrid-reinforcing
777 layers at the last cycle of each applied loading phase, at pipe burial depth of H/D =
778 1.5. It is obvious that inserting geogrid-reinforcing layers remarkably affected the
779 strain value along the invert of the pipe. During the first loading phase, the strain
780 value decreased with 6% and 12.6% due to inserting one and two geogrid-layers,
781 respectively. This ratio increased gradually with the progression of the applied
782 cyclic loading phases until the application of the fourth loading phase. By reaching
783 the end of the fourth loading phase, the reduction ratio in the values of the invert
784 strain was 23.9% and 40.1% for one and two geogrid-layers, respectively. Such
785 increase in the reduction ratios could be attributed to the end of the slack effect of
786 the geogrid-reinforcing layers, as well as the occurred enhancement in the
787 generated load transfer mechanisms between the geogrid-layers and the trapped
788 soil between its apertures, particularly the passive earth resistance mechanism.
789 Due to the application of the fifth and the seventh cyclic loading phases, the
790 unreinforced system and the reinforced system using one-geogrid layer,
791 respectively, failed to sustain additional load, as presented in Fig. 11.
792 Consequently, it is clear that the inclusion of the geogrid-reinforcing layers
793 contributed significantly to decreasing the strain values generated along the invert

Satu Niemi
Formatted
CS

Satu Niemi
Deleted:

Satu Niemi
Formatted
CS, Not Ita
grammar

Satu Niemi
Formatted
CS

Satu Niemi
Formatted
CS, Not Ita
grammar

Satu Niemi
Deleted:

Satu Niemi
Formatted
CS, Not Ita
grammar

Satu Niemi
Deleted:

Satu Niemi
Formatted
CS

of the pipe, where lower value of the applied pressure was transferred to the pipe due to the generated load transfer mechanisms. This is in harmony with the observed reduction in the pressure values measured along the crown of the pipe, Fig. 7, and the reduction in the settlement values of the footing, Fig. 3.

It should be noted that at deeper burial depths, similar behaviour was observed, however, the strain values were considerably lower than those measure at shallow burial depth of H/D=1.5. This presents the influence of increasing the burial depth of the pipe, which contribute to decreasing the transferred pressure value to the pipe, which by turn results in a decrease in the strain generated in the pipe.

Crown strain

The strain generation pattern along the crown of the pipe was similar to that observed along its invert, Fig. 11; however, it experienced lower values due to the stress concentration zone that formed between the invert and the bedding layer, in addition to the insignificant deformable nature of the pipe material, which is in agreement with the findings of [20]. This behaviour demonstrated that the pipe burial depth and the number of reinforcing layers significantly influenced the value and rate of the strain in the pipe crown. Fig. 13 illustrates the strain values on the crown of the pipe once reaching the final cycle of each applied loading phase while increasing the pipe burial depth in Series B. During the 1st loading phase, the measured strain values were 0.397%, 0.02% and 0.014% at burial depths of 1.5, 2 and 2.5, respectively. Reduction ratios of 94.96% and 96.37% were observed at *H/D*=2 and 2.5, respectively, compared with *H/D*=1.5, which could be attributed to the reduction in the pressure transferred along the crown of the pipe at deeper

Satu Niemi Deleted:
Satu Niemi Formatted CS
Satu Niemi Deleted:
Satu Niemi Formatted CS, Not Ita grammar
Satu Niemi Formatted CS
Satu Niemi Formatted CS, Not Ita grammar
Satu Niemi Formatted CS, Not Ita grammar
Satu Niemi Deleted:
Satu Niemi Formatted CS
Satu Niemi Formatted CS
Satu Niemi Formatted CS, Not Ita grammar
Satu Niemi Deleted:

burial depths, as presented in Fig. 6. Since the reduction ratio only increased by 1.4% when the burial depth was increased from *H/D*=2 to 2.5, it was concluded that *H/D*=2 could be considered to be an optimum burial depth of the pipe. In addition, the strain reduction rate became more obvious while applying further loading phases. This behaviour controlled the strain along the crown of the pipe until reaching the 5th phase for *H/D*=1.5, and the 7th phase for *H/D*=2 and 2.5, where failure occurred due to excessive footing settlement as illustrated in Fig. 3. As observed in the strain along the pipe invert, the pattern of strain along the crown of the pipe during the 1st loading phase at a shallow burial depth experienced two different rates, particularly at the 300th cycle. This could be attributed to the ending of the reinforcing layer slack effect.

In Series C, similar strain behaviour was recorded for the strain along the crown of the pipe, but with reduced values. This could be attributed to the inclusion of two reinforcing layers, which allowed the generation of an enhanced membrane mechanism and an improved degree of the lateral support, which was provided to the pipe. Consequently, the increase in the pipe burial depth and the number of reinforcing layers significantly decreased the strain along the pipe crown.

Spring-line strain

Fig. 14 demonstrated measured data for strain generated along the pipe spring-line while increasing the applied loading phases, for Series B and C. It is obvious that the spring-line strain pattern is similar to that generated along the pipe crown, Fig. 13, and invert, Fig. 11, but with a significantly reduced scale. This can be attributed to the inclusion of the reinforcing layers, which led to a pressure

Satu Niemi: Formatted CS
Satu Niemi: Deleted:
Satu Niemi: Formatted CS, Not Ita grammar
Satu Niemi: Formatted CS
Satu Niemi: Formatted CS, Not Ita grammar
Satu Niemi: Deleted:
Satu Niemi: Formatted CS, Not Ita grammar
Satu Niemi: Deleted:
Satu Niemi: Formatted CS
Satu Niemi: Formatted CS
Satu Niemi: Formatted CS, Not Ita grammar
Satu Niemi: Deleted:
Satu Niemi: Formatted CS
Satu Niemi: Formatted CS, Not Ita grammar
Satu Niemi: Deleted:

redistribution process over the adjacent soil portions to the pipe, allowing an increase in the lateral support provided to the pipe, particularly its spring-line, i.e. formation of a confined zone. On the other hand, the increased burial depth enabled the existence of a larger soil volume with a larger self-weight, providing extra lateral support. An unexpected decay in the spring-line strain behaviour during *T4* was observed. Visual inspection of the pipe, after testing, indicated the generation of two cracks along the pipe spring-line, where the 1st crack intersected with the strain gauge and the 2nd one did not, as presented in Fig. 15. Concrete tensile failure can be defined by crack formation, where higher values of tensile strain are represented by wider cracks. It was noticed that the 2nd crack was wider than the 1st one. Consequently, the actual values of the tensile strains along the pipe spring-line were not recorded, since the 2nd crack did not intersect with the strain gauge. This explained the obvious decay in the strain values along the pipe spring-line in *T4*.

8.2.7 Reinforcing layers strain

Fig. 16 showed the tensile strain generated in the geogrid-layer as a result of increasing the applied cyclic loading phases, in Series B, where one geogrid-layer was utilised to enhance the backfill performance. At the same cyclic load, it was observed that the increase of the pipe burial depth negatively influenced the tensile strain generated in the geogrid-layer, where its value increased, unlike the strain values measured along the pipe different sections, pressure transferred to the crown of the pipe, and the measured footing settlement. The location of the pipe contributed to the system stability, where system stability became less

Satu Niemi
Formatted
CS

Satu Niemi
Formatted
CS, Not Ita
grammar

Satu Niemi
Deleted:

Satu Niemi
Formatted
CS

Satu Niemi
Formatted
CS, Not Ita
grammar

Satu Niemi
Deleted:

dependent on the pipe at deep burial depths and the strain along the wall of the pipe was significantly reduced, as shown in Fig. 11 and Fig. 14. At this stage, the stability of the system was gradually dominated by the reinforcing layers, where the tensile strain values were significantly increased. This behaviour became apparent at and after a pipe burial depth of *H/D*=2. It should be noted that the trapped soil volume between the soil surface and the pipe could be divided into upper and lower zones. As a result of the high stiffness of the pipe, it significantly contributed to reinforcing the lower zone but it paid a lower contribution to the stability of the upper zone. At deep burial depths, soil properties dominated the upper zone stability, where the tensile strain value increased and the existence of the reinforcing layer became crucial in sustaining the tensile strains. Consequently, the inclusion of reinforcing layers maintained the upper zone stability. It should be noted that the distance between the reinforcement and the pipe controlled the contribution of each of them to the upper zone stability, where the reinforcing layer had a major contribution if it was located far from the pipe.

The strain generation rate depended on the slack effect of the reinforcing layers, as shown in Fig. 16. Within the first 300 cycles of the 1st phase of loading, the strain generation rate was fast as the slack effect progressed, and with the progression of loading cycles, the rate decreased significantly as no further slack effect occurred [2, 79, 80]. Based on the applied loading profile, the tensile strain in the reinforcing layer gradually increased, where this increase became very rapid once system failure began despite the applied load and the pipe burial depth. Visual inspection of the reinforcing layers after testing illustrated permanent

Satu Niemi
Formatted
CS

Satu Niemi
Deleted:

Satu Niemi
Formatted
CS, Not Ita
grammar

Satu Niemi
Formatted
CS

Satu Niemi
Formatted
CS, Not Ita
grammar

Satu Niemi
Deleted:

Satu Niemi
Formatted
CS, Not Ita
grammar

Satu Niemi
Deleted:

Satu Niemi
Formatted
CS

deformation but no damage was observed. Eventually, the stability of the reinforced pipe-soil system was enhanced with the increase of the burial depth of the pipe, where the reinforcing layer endured the tensile strain.

In Series C, to achieve an enhanced degree of system stability and additional protection to the pipe, two layers of reinforcement were utilized, to carry the tensile strains. Fig. 17 shows the tensile strain in the reinforcing layers in relation to both burial depth and applied loading cycles. After testing, the soil cover above the reinforcing layers was carefully removed, and their deformations were inspected. Usually, the deformation of the upper layer was higher than the lower one. Since the upper layer was closer to the footing, more pressure was transferred to it, while less pressure was transferred to the lower layer. However, Fig. 18 illustrates that the value of the tensile strain sustained by the lower layer was higher than that sustained by the upper one, despite the loading phase and the pipe burial depth, which was a good match with the findings of Jones and Cooper [83] and Elshesheny, Mohamed [2].

This behaviour illustrated that a stiff platform was formed out of the two utilised layers of reinforcements and the trapped soil layer between them, which behaved as a flexible reinforced slab, which is a good match with the findings of Mohamed [84]. Due to the applied load, bending stresses were generated in the stiff platform, significantly influencing the lower layer of reinforcement, and generating tensile and compressive strains along the lower and upper surfaces respectively of the stiff platform that had formed. Therefore, the entire system stability and performance were dominated by the tensile strain sustained by the lower layer of

Satu Niemi
Formatted
CS

Satu Niemi
Formatted
CS, Not Ita
grammar

Satu Niemi
Deleted:

Satu Niemi
Formatted
CS

Satu Niemi
Formatted
CS, Not Ita
grammar

Satu Niemi
Deleted:

928 reinforcement. It should be noted that failure of the reinforcing layer was controlled
929 by the sustained value of the tensile strain rather than the deformation that
930 occurred. The reinforcing layers did not suffer any creep deformation, which could
931 be attributed to the nature of the loading, since no prolonged loading was applied.

932 ## 9 CONCLUSIONS

933 The performance of buried rigid pipes underneath geogrid-reinforced soil while
934 applying incrementally increased cyclic loading was experimentally investigated
935 using a fully instrumented laboratory rig, where results were compared with
936 controlled tests on unreinforced sand beds [63]. Based on the results of this
937 research, the following conclusions can be drawn;

938 1. The location of the pipe inside the system controlled the values of the
939 stresses and strains along its walls.
940 2. The inclusion of the geogrid-layers in the tested systems allowed a stress
941 redistribution process, which led to the formation of a confined zone around
942 the pipe.
943 3. Pressure distribution inside the reinforced-soil system was governed by
944 three mechanisms, i. passive arching, ii. load mitigation and iii. distributed
945 load over reinforcing layer.
946 4. Under applied load, the bedding layer was densified by different degrees
947 according to the pipe burial depth. This led to a stress concentration along
948 the invert of the pipe, generating the maximum tensile strain.
949 5. Rebound of the invert deformation depends on the pressure distribution
950 around the pipe and the densification degree of the bedding layer.

6. The lower reinforcing layer sustained tensile strain higher than that of the upper layer, despite the increased deformation of the upper layer. This could be attributed to the flexible slab that formed, which depended on the configuration of the reinforcing layers.
7. The data measured along the pipe showed that the inclusion of geogrid-reinforcing layers in a rigid pipe-soil system subjected to cyclic loading achieved the ITM principles, where deformations, strains and stresses were reduced.

In this research one type of silica sand and one type of geogrid reinforcing layer were tested, where they were used to prepare the reinforced sand beds in which one type of rigid concrete pipe with a specific diameter was buried at variable depths. Moreover, all of the tests were performed using the same loading profile, where the number of the applied loading phases was found to be dependent on each test condition. Therefore, the findings of this research are limited to the above test conditions.

10 ACKNOWLEDGMENT

The contribution of Tensar International, which provided the geogrid-layers used in this investigation, is highly appreciated.

REFERENCES:

[1] Talesnick, M.L., H.W. Xia, and I.D. Moore, *Earth pressure measurements on buried HDPE pipe.* Geotechnique, 2011. **61**(9): p. 721.

[2] Elshesheny, A., M. Mohamed, and T. Sheehan, *Buried flexible pipes behaviour in unreinforced and reinforced soils under cyclic loading.* Geosynthetics International, 2019. **26**(2): p. 184-205.

[3] Zhou, M., et al., *Performance of buried HDPE pipes–part II: total deflection of the pipe.* Geosynthetics International, 2017. **24**(4): p. 396-407.

[4] Alzabeebee, S., et al. *The response of buried pipes to UK standard traffic loading*. 2017.

[5] Mehrjardi, G.T., S.N.M. Tafreshi, and A.R. Dawson, *Pipe response in a geocell-reinforced trench and compaction considerations.* Geosynthetics International, 2013. **20**(2): p. 105-118.

[6] Corey, R., et al., *Laboratory study on geosynthetic protection of buried steel-reinforced HDPE pipes from static loading.* Journal of Geotechnical and Geoenvironmental Engineering, 2014. **140**(6): p. 04014019.

[7] Wang, F., et al., *Numerical Modeling of Installation of Steel-Reinforced High-Density Polyethylene Pipes in Soil.* Journal of Geotechnical and Geoenvironmental Engineering, 2017. **143**(11): p. 04017084.

[8] Brachman, R.W., I. Moore, and R. Rowe, *The design of a laboratory facility for evaluating the structural response of small-diameter buried pipes.* Canadian Geotechnical Journal, 2000. **37**(2): p. 281-295.

[9] Cao, Z., et al., *Road surface permanent deformations with a shallowly buried steel-reinforced high-density polyethylene pipe under cyclic loading.* Geotextiles and Geomembranes, 2016. **44**(1): p. 28-38.

[10] Mehrjardi, G.T., S.M. Tafreshi, and A. Dawson, *Combined use of geocell reinforcement and rubber–soil mixtures to improve performance of buried pipes.* Geotextiles and Geomembranes, 2012. **34**: p. 116-130.

[11] Hegde, A.M. and T.G. Sitharam, *Experimental and numerical studies on protection of buried pipelines and underground utilities using geocells.* Geotextiles and Geomembranes, 2015. **43**(5): p. 372-381.

[12] Gilley, C.W. and L.H. Gabriel, *Field performance of cast-in-place nonreinforced concrete pipe.* Transportation Research Record, 1993(1415): p. 47-50.

[13] Vaslestad, J., T.H. Johansen, and W. Holm, *Load reduction on rigid culverts beneath high fills: long-term behavior.* Transportation Research Record, 1993: p. 58-58.

[14] McGrath, T.J., E.T. Selig, and M.C. Webb, *Field tests of concrete pipe performance during backfilling*, in *Concrete pipe for the new millennium*, I.E. I. Kaspar, Editor 2000, Special Technical Publications, ASTM SPT-1368. p. 73-88.

[15] Wong, L.S., et al., *Long-term monitoring of SIDD Type IV installations.* Canadian geotechnical journal, 2006. **43**(4): p. 392-408.

[16] Lay, G. and R. Brachman, *Full-scale physical testing of a buried reinforced concrete pipe under axle load.* Canadian geotechnical journal, 2014. **51**(4): p. 394-408.

[17] Rakitin, B. and M. Xu, *Centrifuge modeling of large-diameter underground pipes subjected to heavy traffic loads.* Canadian Geotechnical Journal, 2013. **51**(4): p. 353-368.

[18] Sheldon, T., H. Sezen, and I.D. Moore, *Joint response of existing pipe culverts under surface live loads.* Journal of Performance of Constructed Facilities, 2013. **29**(1): p. 04014037 1-9.

[19] Peter, J.M., et al., *Impact of soil erosion voids on reinforced concrete pipe responses to surface loads.* Tunnelling and Underground Space Technology, 2018. **82**: p. 111-124.
[20] Abolmaali, A. and A. Kararam, *Nonlinear finite-element-based investigation of the effect of bedding thickness on buried concrete pipe.* Journal of Transportation Engineering, 2010. **136**(9): p. 793-799.
[21] Abolmaali, A. and A. Kararam, *Nonlinear finite-element modeling analysis of soil-pipe interaction.* International Journal of Geomechanics, 2011. **13**(3): p. 197-204.
[22] Kraus, E., J. Oh, and E.G. Fernando, *Impact of repeat overweight truck traffic on buried utility facilities.* Journal of Performance of Constructed Facilities, 2013. **28**(4): p. 04014004.
[23] Alzabeebee, S., et al. *The response of buried pipes to UK standard traffic loading*. in *Proc. Inst. Civ. Eng. Geotech. Eng*. 2017.
[24] Alzabeebee, S., et al. *Investigating the maximum soil pressure on a concrete pipe with poor haunch support subjected to traffic live load using numerical modelling*. in *in Proceedings of the 11th Pipeline Technology Conference*. 2016. Berlin, Germany.
[25] Meguid, M.A. and S. Kamel, *A three-dimensional analysis of the effects of erosion voids on rigid pipes.* Tunnelling and Underground Space Technology, 2014. **43**: p. 276-289.
[26] Ni, P., X. Qin, and Y. Yi, *Numerical study of earth pressures on rigid pipes with tire-derived aggregate inclusions.* Geosynthetics International, 2018: p. 1-45.
[27] Nagy, N., M. Mohamed, and J.C. Boot, *Nonlinear numerical modelling for the effects of surface explosions on buried reinforced concrete structures.* Geomechanics and Engineering, 2010. **2**(1): p. 1-18.
[28] Kim, H., B. Choi, and J. Kim, *Reduction of earth pressure on buried pipes by EPS geofoam inclusions.* Geotechnical Testing Journal, 2010. **33**(4): p. 304-313.
[29] Kim, J., et al. *Experimental study on the behavior of segmented buried concrete pipelines subject to ground movements*. in *in Proceedings of SPIE Nondestructive Characterization for Composite Materials, Aerospace Engineering, Civil Infrastructure, and Homeland Security*. 2009. International Society for Optics and Photonics.
[30] Anderson, A.O., *The theory of loads on pipes in ditches: and tests of cement and clay drain tile and sewer pipe*. Vol. 31. 1913, Ames, Iowa: Iowa State College of Agriculture and Mechanic Arts.
[31] Spangler, M.G., *The supporting strength of rigid pipe culverts*. Vol. 112. 1933: Iowa State College.
[32] Rogers, C., P. Fleming, and R. Talby, *Use of visual methods to investigate influence of installation procedure on pipe-soil interaction.* Transportation Research Record: Journal of the Transportation Research Board, 1996(1541): p. 76-85.
[33] Marston, A., *Second progress report to the joint concrete culvert pipe committee.* Iowa Engineering Experimental Station, Ames, IA, 1922.
[34] Marston, A. *The theory of external loads on closed conduits in the light of the latest experiments*. in *Highway Research Board Proceedings*. 1930.
[35] Spangler, M.G., *A theory on loads on negative projecting conduits.* Proceedings of the Highway Research Board, 30, Transportation Research Board, Washington, DC, 1950. **30**: p. 153–161.
[36] Spangler, M.G., *A practical application of the imperfect ditch method of construction.* Highway Research Board Proceedings, 1958. **37**.

[37] Larsen, N.G. and J.G. Hendrickson, *A practical method for constructing rigid conduits under high fills.* Highway Research Board Proceedings, 1962. **41**.
[38] McAffee, R.P. and A.J. Valsangkar, *Geotechnical properties of compressible materials used for induced trench construction.* Journal of Testing and Evaluation, 2004. **32**(2): p. 143-152.
[39] Meguid, M.A., et al., *Investigation of soil-geosynthetic-structure interaction associated with induced trench installation.* Geotextiles and Geomembranes, 2017. **45**(4): p. 320-330.
[40] Turan, A., M.H. El Naggar, and D. Dundas, *Investigation of induced trench method using a full scale test embankment.* Geotechnical and Geological Engineering, 2013. **31**(2): p. 557-568.
[41] McAffee, R.P. and A.J. Valsangkar, *Field performance, centrifuge testing, and numerical modelling of an induced trench installation.* Canadian Geotechnical Journal, 2008. **45**(1): p. 85-101.
[42] Bartlett, S.F. and B.N. Lingwall, *Protection of Pipelines and Buried Structures Using EPS Geofoam*, in *Ground Improvement and Geosynthetics*2014. p. 547-556.
[43] Meguid, M.A. and T.A. Youssef, *Experimental investigation of the earth pressure distribution on buried pipes backfilled with tire-derived aggregate.* Transportation Geotechnics, 2018. **14**: p. 117-125.
[44] Bartlett, S.F., B.N. Lingwall, and J. Vaslestad, *Methods of protecting buried pipelines and culverts in transportation infrastructure using EPS geofoam.* Geotextiles and Geomembranes, 2015. **43**(5): p. 450-461.
[45] Witthoeft, A.F. and H. Kim, *Numerical investigation of earth pressure reduction on buried pipes using EPS geofoam compressible inclusions.* Geosynth Int, 2016. **23**(4): p. 1-14.
[46] Xu, C., C. Liang, and P. Shen, *Experimental and theoretical studies on the ultimate bearing capacity of geogrid-reinforced sand.* Geotextiles and Geomembranes, 2019.
[47] Bathurst, R.J. and F.M. Ezzein, *Insights into geogrid–soil interaction using a transparent granular soil.* Géotechnique Letters, 2017. **7**(2): p. 179-183.
[48] Vangla, P. and M.L. Gali, *Effect of particle size of sand and surface asperities of reinforcement on their interface shear behaviour.* Geotextiles and Geomembranes, 2016. **44**(3): p. 254-268.
[49] Pinho-Lopes, M., A.M. Paula, and M.d.L. Lopes, *Pullout response of geogrids after installation.* Geosynthetics International, 2015. **22**(5): p. 339-354.
[50] Tran, V.D.H., M.A. Meguid, and L.E. Chouinard, *Three-dimensional analysis of geogrid-reinforced soil using a finite-discrete element framework.* International Journal of Geomechanics, 2014. **15**(4): p. 04014066.
[51] Zhou, J., et al., *Micro-mechanism of the interaction between sand and geogrid transverse ribs.* Geosynthetics International, 2012. **19**(6): p. 426-437.
[52] Ferellec, J.F. and G.R. McDowell, *Modelling of ballast–geogrid interaction using the discrete-element method.* Geosynthetics International, 2012. **19**(6): p. 470-479.
[53] Latha, G.M. and A. Somwanshi, *Bearing capacity of square footings on geosynthetic reinforced sand.* Geotextiles and Geomembranes, 2009. **27**(4): p. 281-294.
[54] Wang, J.-Q., et al., *Load-settlement response of shallow square footings on geogrid-reinforced sand under cyclic loading.* Geotextiles and Geomembranes, 2018. **46**(5): p. 586-596.

[55] Venkateswarlu, H., K.N. Ujjawal, and A. Hegde, *Laboratory and numerical investigation of machine foundations reinforced with geogrids and geocells.* Geotextiles and Geomembranes, 2018. **46**(6): p. 882-896.
[56] Mousavi, S.H., M.A. Gabr, and R.H. Borden, *Optimum location of geogrid reinforcement in unpaved road.* Canadian Geotechnical Journal, 2017. **54**(7): p. 1047-1054.
[57] Tafreshi, S.N.M. and A.R. Dawson, *Behaviour of footings on reinforced sand subjected to repeated loading–Comparing use of 3D and planar geotextile.* Geotextiles and Geomembranes, 2010. **28**(5): p. 434-447.
[58] Mehrjardi, G.T., S.M. Tafreshi, and A. Dawson, *Pipe response in a geocell-reinforced trench and compaction considerations.* Geosynthetics International, 2013. **20**(2): p. 105-118.
[59] Asakereh, A., S.N.M. Tafreshi, and M. Ghazavi, *Strip footing behavior on reinforced sand with void subjected to repeated loading.* International Journal of Civil Engineering, 2012. **10**(2): p. 139-152.
[60] Tafreshi, S.M. and O. Khalaj, *Laboratory tests of small-diameter HDPE pipes buried in reinforced sand under repeated-load.* Geotextiles and Geomembranes, 2008. **26**(2): p. 145-163.
[61] El Naggar, H., A. Turan, and A. Valsangkar, *Earth pressure reduction system using geogrid-reinforced platform bridging for buried utilities.* Journal of Geotechnical and Geoenvironmental Engineering, 2015. **141**(6): p. 04015024.
[62] Ahmed, M., V. Tran, and M. Meguid, *On the role of geogrid reinforcement in reducing earth pressure on buried pipes: experimental and numerical investigations.* Soils and Foundations, 2015. **55**(3): p. 588-599.
[63] Elshesheny, A., M. Mohamed, and T. Sheehan, *Performance of buried rigid pipes under the application of incrementally increasing cyclic loading.* Soil Dynamics and Earthquake Engineering, 2019. **125**: p. 1-13.
[64] Hussein, M. and M. Meguid, *A three-dimensional finite element approach for modeling biaxial geogrid with application to geogrid-reinforced soils.* Geotextiles and Geomembranes, 2016. **44**(3): p. 295-307.
[65] Hussein, M.G., et al., *On the numerical modeling of buried structures with compressible inclusion.* GeoQuebec, September, Quebec City, 2015. **8**.
[66] Arockiasamy, M., O. Chaallal, and T. Limpeteeprakarn, *Full-scale field tests on flexible pipes under live load application.* Journal of performance of constructed facilities, 2006. **20**(1): p. 21-27.
[67] Perkins, S. and M. Edens, *Finite element modeling of a geosynthetic pullout test.* Geotechnical & Geological Engineering, 2003. **21**(4): p. 357-375.
[68] BS, *BS1377-1, Methods of test for soils for civil engineering purposes – Part 1: General requirements and sample preparation*, 2016, British Standards Institution: London, UK.
[69] Lambe, T.W. and R.V. Whitman, *Soil mechanics*. Vol. 10. 1991: John Wiley & Sons.
[71] Moser, A.P. and S.L. Folkman, *Buried pipe design*. 2nd Ed2001, USA: McGraw-Hill New York.
[72] BS, *BS EN 12390-3:2009 - Testing hardened concrete - Part 3: Compressive strength of test specimens*, 2009, British Standards Institution: London, UK.
[73] BS, *BS EN ISO 10319, Geosynthetics — Wide-width tensile test*, 2015, British Standards Institution: London.
[74] BS, *NA to BS EN 1991-2, UK National Annex to Eurocode 1: Actions on structures - Part 2: Traffic loads on bridges*, 2003, British Standards Institution: London, UK.

[75] Mehrjardi, G.T. and S.M. Tafreshi. *Buried pipes analysis in reinforced sand under repeated loading*. in *Proceedings of the Second BGA International Conference on Foundations, ICOF2008, Dundee, UK*. 2008.
[76] Mir Mohammad, S. and S. Moghaddas Tafreshi, *Soil-structure interaction of buried pipes under cyclic loading conditions.* International Journal of Engineering-Transactions B: Applications, 2001. **15**(2): p. 117.
[77] Terzaghi, K. and R.B. Peck, *Soil mechanics in engineering practice*. 2nd edn1967, New York: John Wiley & Sons. 729.
[78] Young, O.C. and J.J. Trott, *Buried Rigid Pipes: Structural Design of Pipelines*1984, London: Elsevier Applied Science Publishers. 229.
[79] Chenggang, B., *Study on the interaction behavior of geosynthetics and soil in China.* Ningbo Institute of Technology, Zhejiang University, China, 2004.
[80] Sieira, A.C.C., D.M. Gerscovich, and A.S. Sayao, *Displacement and load transfer mechanisms of geogrids under pullout condition.* Geotextiles and Geomembranes, 2009. **27**(4): p. 241-253.
[81] Tran, V., M. Meguid, and L. Chouinard, *A finite–discrete element framework for the 3D modeling of geogrid–soil interaction under pullout loading conditions.* Geotextiles and Geomembranes, 2013. **37**: p. 1-9.
[82] Abu-Farsakh, M., Q. Chen, and R. Sharma, *An experimental evaluation of the behavior of footings on geosynthetic-reinforced sand.* Soils and Foundations, 2013. **53**(2): p. 335-348.
[83] Jones, C.J. and A.H. Cooper, *Road construction over voids caused by active gypsum dissolution, with an example from Ripon, North Yorkshire, England.* Environmental Geology, 2005. **48**(3): p. 384-394.
[84] Mohamed, M.H., *Two dimensional experimental study for the behaviour of surface footings on unreinforced and reinforced sand beds overlying soft pockets.* Geotextiles and Geomembranes, 2010. **28**(6): p. 589-596.
[85] Tensar, I., *Tensar SS Geogrids Product Specifications*, 2012.

List of Tables:

1204 Table 1: Properties of the silica sand used

Test	Description	Value
Sieve analysis	Coefficient of uniformity, C_u	1.3
	Coefficient of curvature, C_c	1.0
	Effective grain size, D_{10} (mm)	0.5
	D_{30} (mm)	0.6
	Medium grain size, D_{50} (mm)	0.6
	D_{60} (mm)	0.7
Standard Proctor	Proctor dry unit weight (kN/m^3)	16.4
	Optimum water content %	7.9
	Maximum dry unit weight (kN/m^3)	17.1
	Minimum dry unit weight (kN/m^3)	15.3
	Maximum void ratio, e_{max}	0.7
	Minimum void ratio, e_{min}	0.5
	Relative density, D_r (%)	57.0
	Specific gravity, G_s	2.6
	Actual unit weight of sand (kN/m^3)	16.32
Shear box and Triaxial	Stiffness considering initial tangent modulus (kN/m^2)	55000.0
	Stiffness considering secant modulus from zero to 50 % of the peak deviator stress (kN/m^2)	54000.0
	Friction angle (degree), Φ	36.5
	Cohesion (kN/m^2), c	0.0

1205

1206

1207

1208 Table 2: Mechanical properties of the reinforcing layers

Description	Value	Source
Material	Polypropylene	Manufacturer,
Aperture size (mm)	39.0 x 39.0	[85]
Thickness (mm)	1.1	
Weight/unit area (kN/m^2)	0.00216	
Ultimate tensile strength, T_{ult} (kN/m)	20.0	
Load at 2% strain (kN/m)	7.0	
Load at 5% strain (kN/m)	14.0	
Strain at T_{ult} (%)	11.0	
Elements unit weight (kN/m^3)	2.7	Tensile Test,
Elastic modulus (kN/m^2)	300000.0	[73]

1209

1210

1211 Table 3: Value of the applied cyclic loading phases

Test series			Load phase	Mean load (kN)	Load range (kN)		Amplitude (kN)
					Min.	Max.	
Series A (5 load phases)			Phase 1	13	8	18	5
			Phase 2	18	13	23	5
			Phase 3	23	18	28	5
			Phase 4	28	23	33	5
			Phase 5	33	28	38	5
	Series B (8 load phases)		Phase 6	38	33	43	5
			Phase 7	43	38	48	5
			Phase 8	48	43	53	5
		Series C (12 load phases)	Phase 9	53	48	58	5
			Phase 10	58	53	63	5
			Phase 11	63	58	68	5
			Phase 12	68	63	73	5

1212

1213

1214 Table 4: Testing program

Test series	Test type	Tests	Test configuration					Tests No.
			RFT. No.	*u/B*	*h/B*	*L/B*	*H/D*	
A	Unreinforced case	*T1:T3*	-	-	-	-	1.5, 2, 2.5	3
B	Reinforced case	*T4:T6*	1	0.35	0.35	5	1.5, 2, 2.5	3
C		*T7:T9*	2	0.35	0.35	5	1.5, 2, 2.5	3
D	Repetition of *T4*	*T10*	1	0.35	0.35	5	1.5	1

1215 Note: *RFT* refers to reinforcing layer; *u* stands for the spacing between topmost
1216 reinforcing layer and footing; *B* is the footing width; *h* is the spacing between
1217 reinforcing layers; *L* denotes reinforcement length; *H* is the pipe burial depth from
1218 ground surface; *D* is the outer diameter of the pipe.

1219

List of Figures:

1243

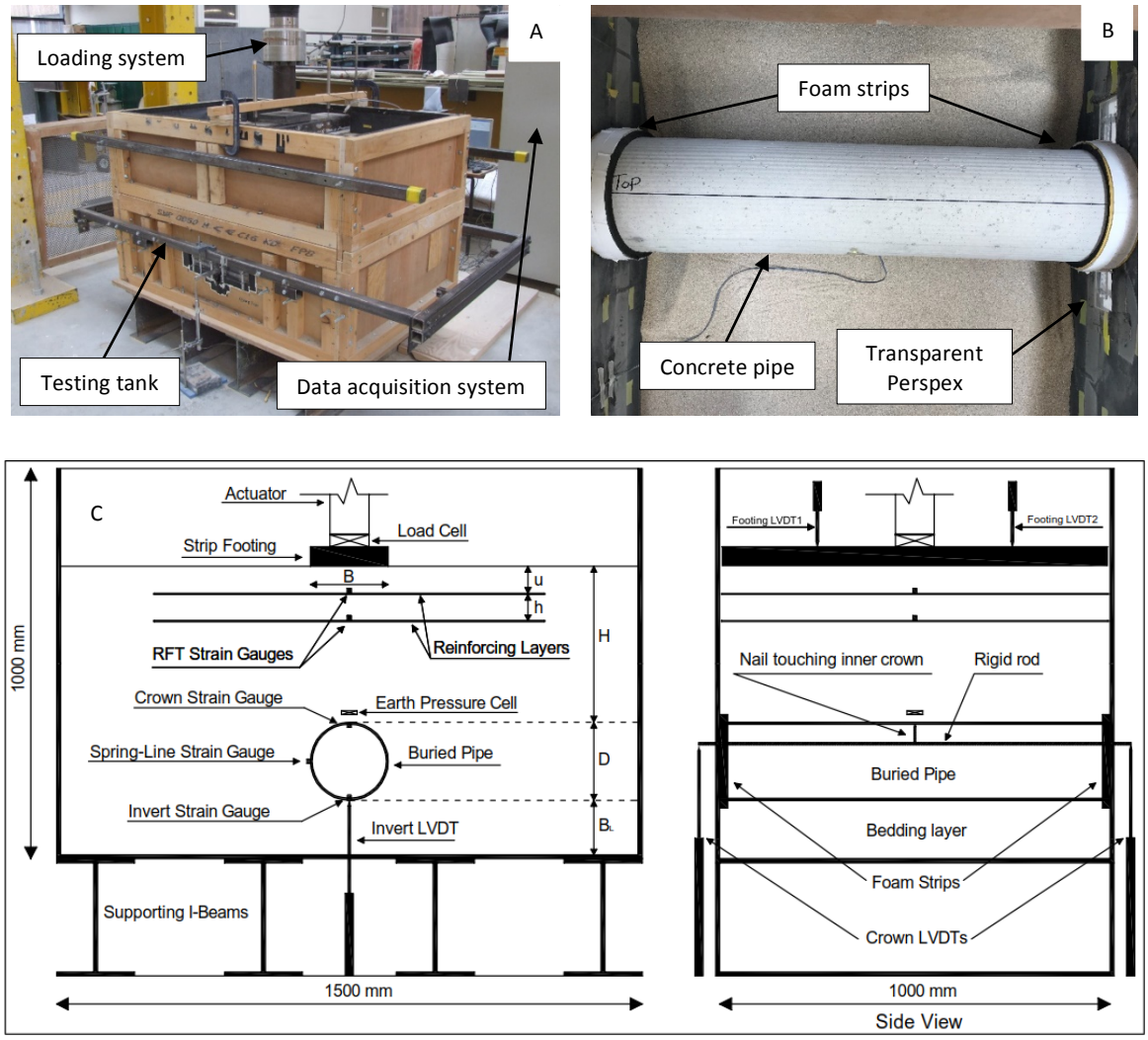

Fig. 1 Testing rig and measuring instruments

A: Testing rig. B: Concrete pipe. C: Schematic diagram of testing rig.

1244

1245

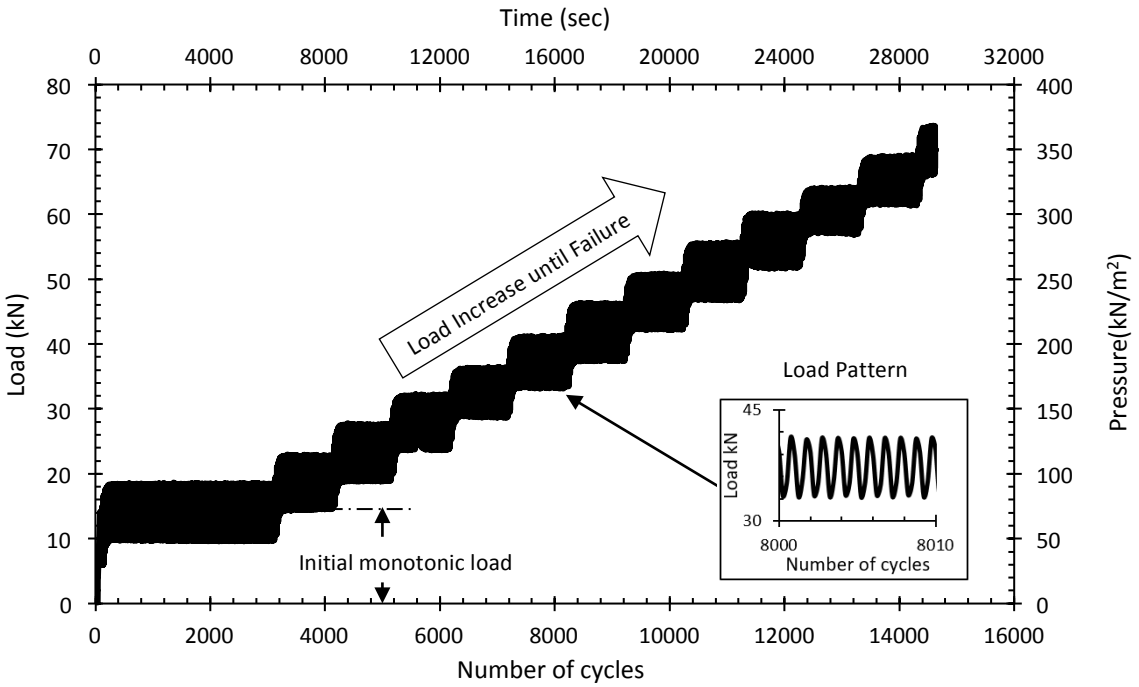

Fig. 2 Applied load profile

1246

1247

1248

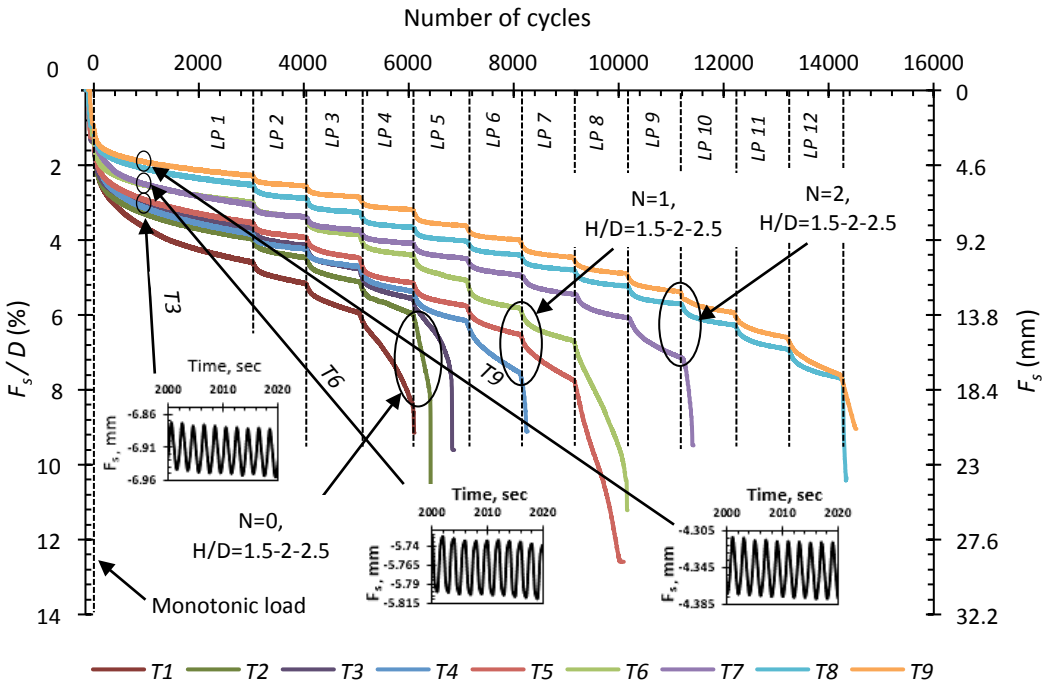

Fig. 3 Footing settlement ratio against number of cycles

1249

1250

1251

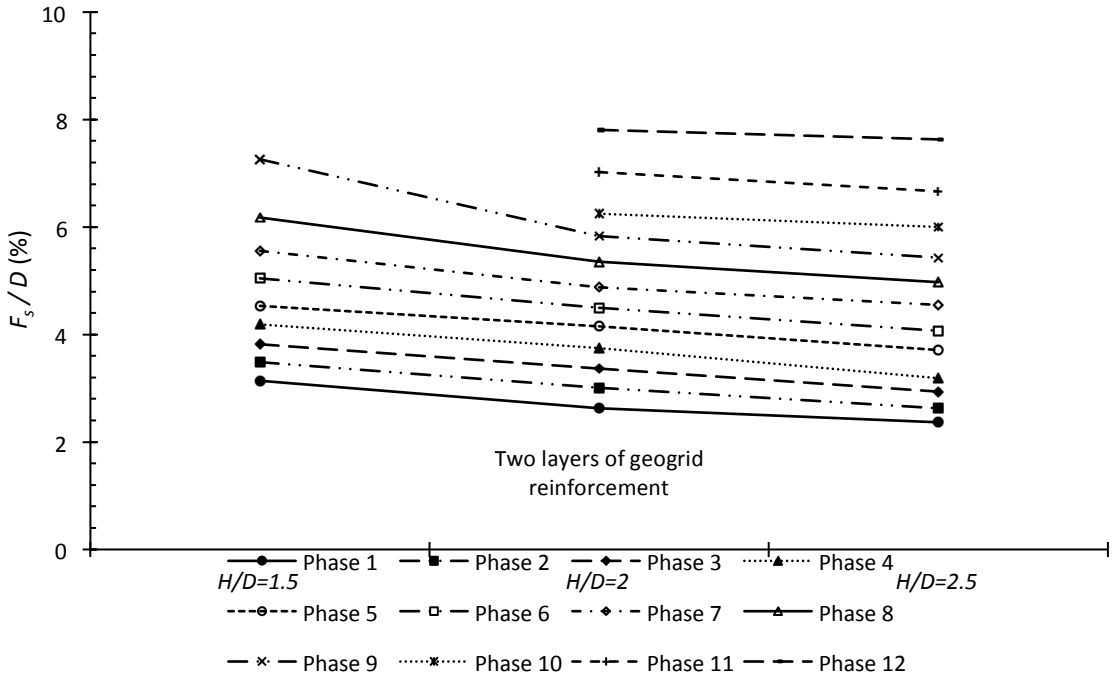

Fig. 4 Footing settlement with loading phase progression, Series C

1252

1253

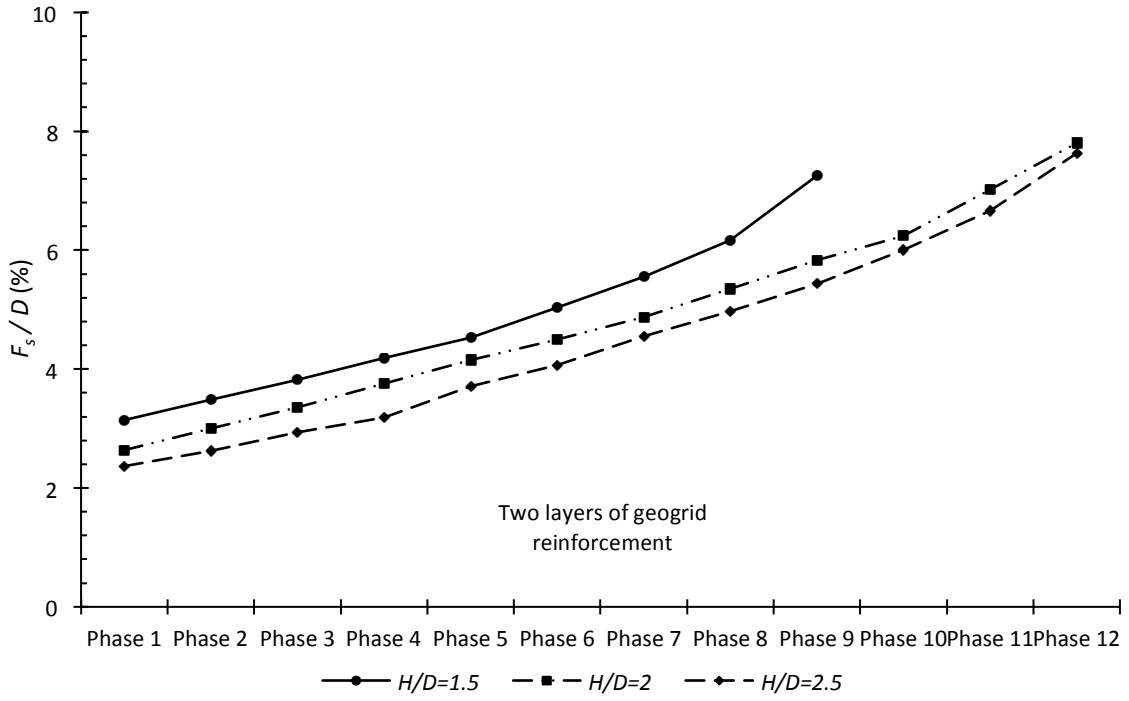

Fig. 5 Change in footing settlement rate, Series C

1254

1255

1256

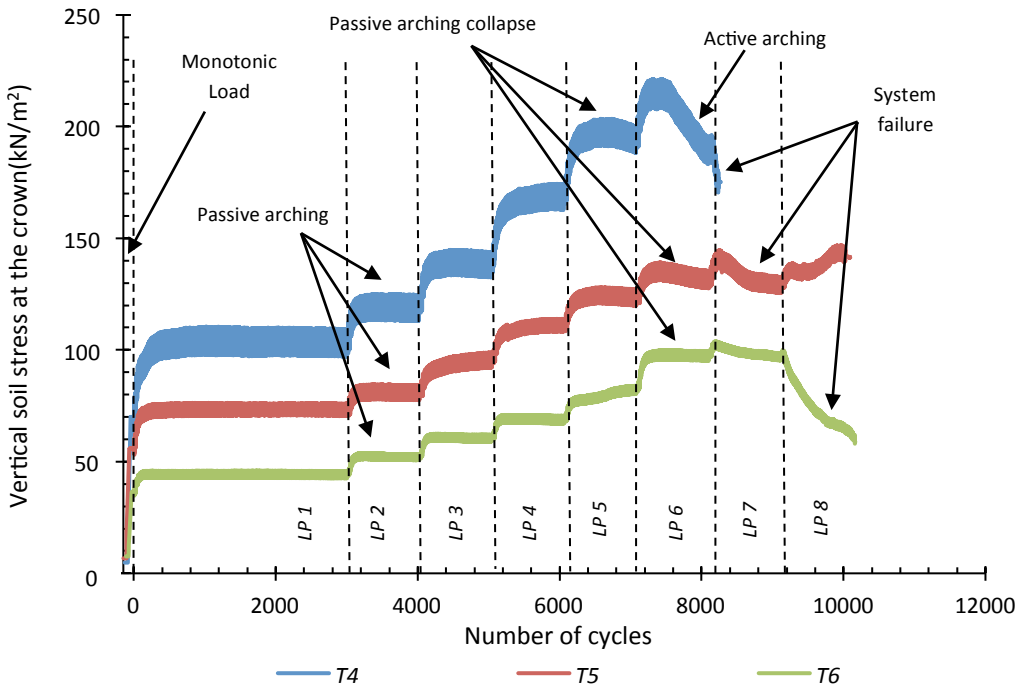

Fig. 6 Pressure on the pipe against number of cycles, Series B

1257

1258

1259

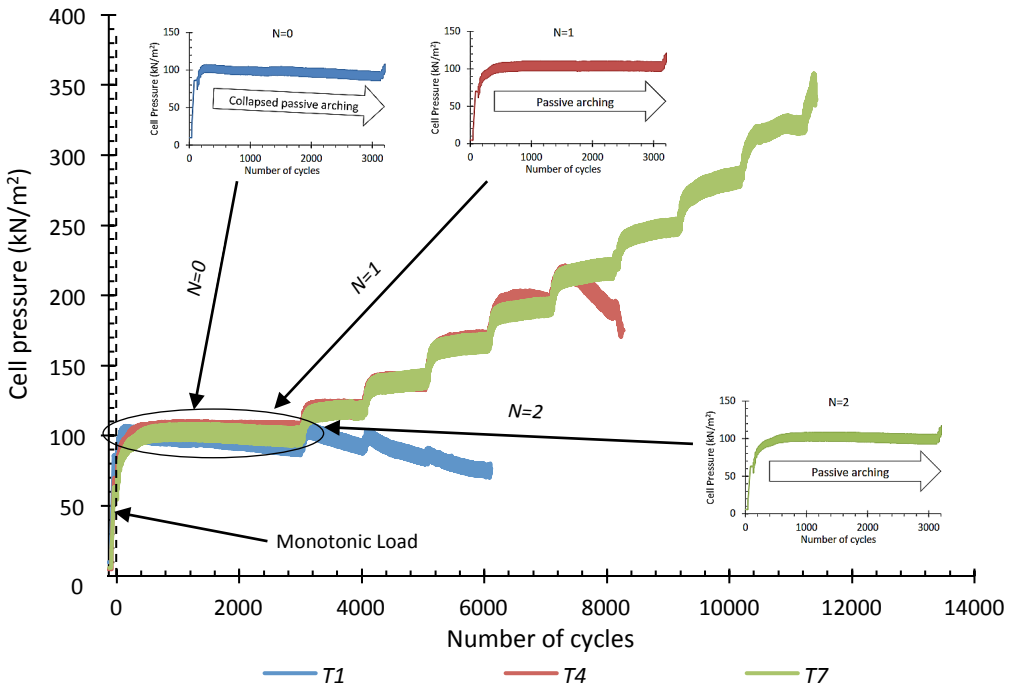

Fig. 7 Effect of reinforcing layer inclusion on the pressure at H/D=1.5

1260

1261

1262

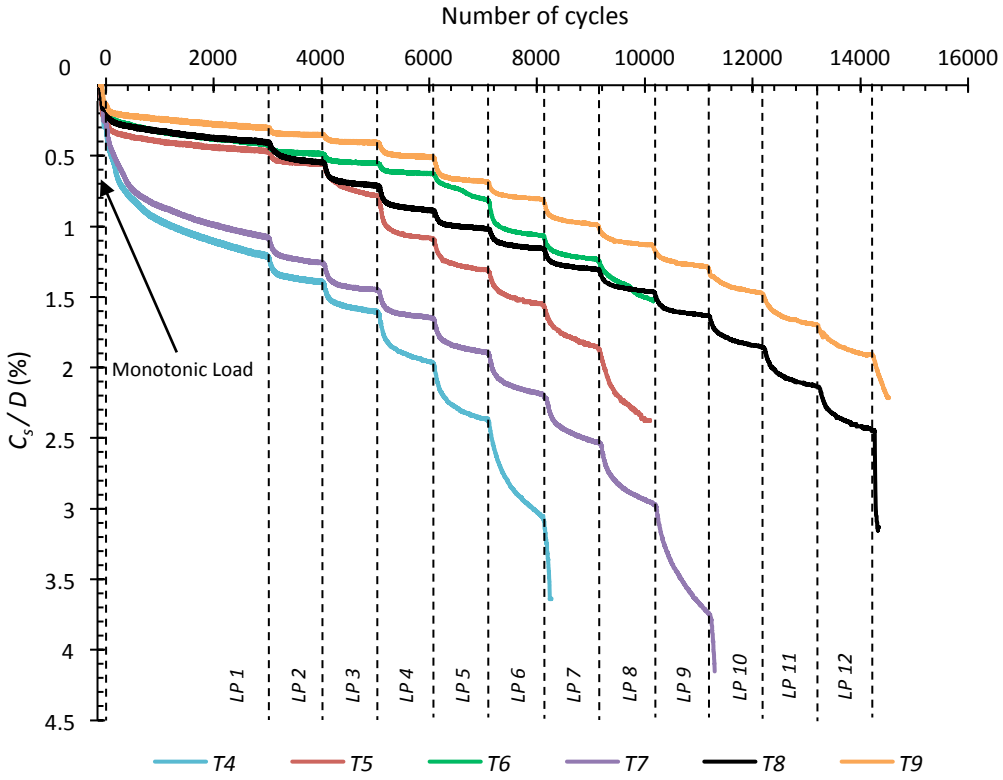

Fig. 8 Normalised crown settlement with loading phase progression

1263

1264

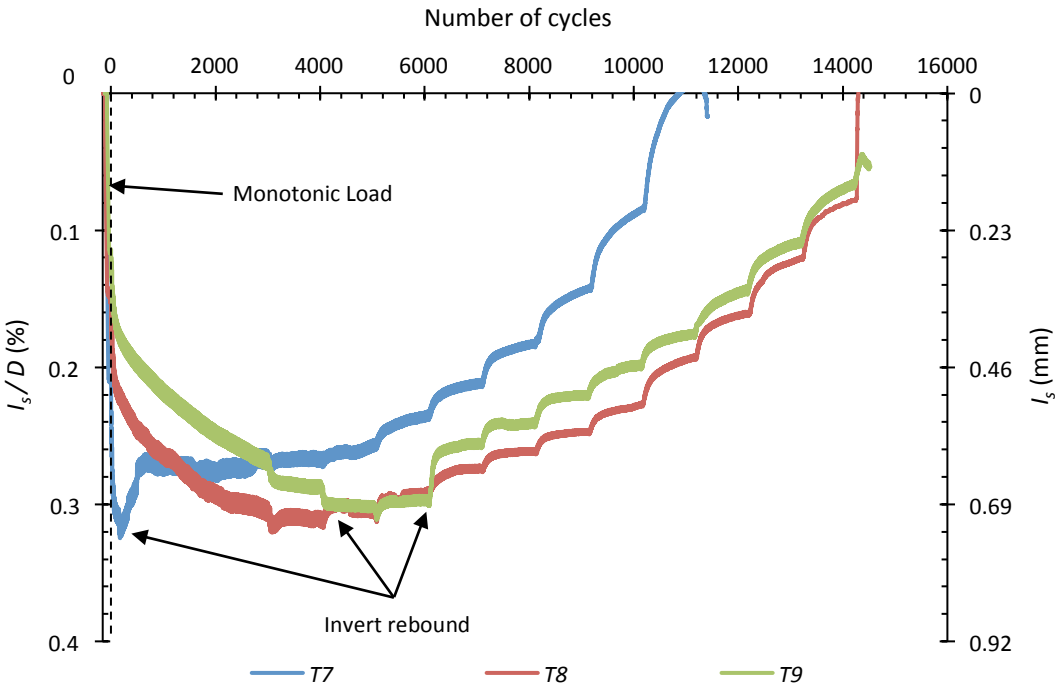

Fig. 9 Invert deformation due to loading phase progression, Series C

1265

1266

1267

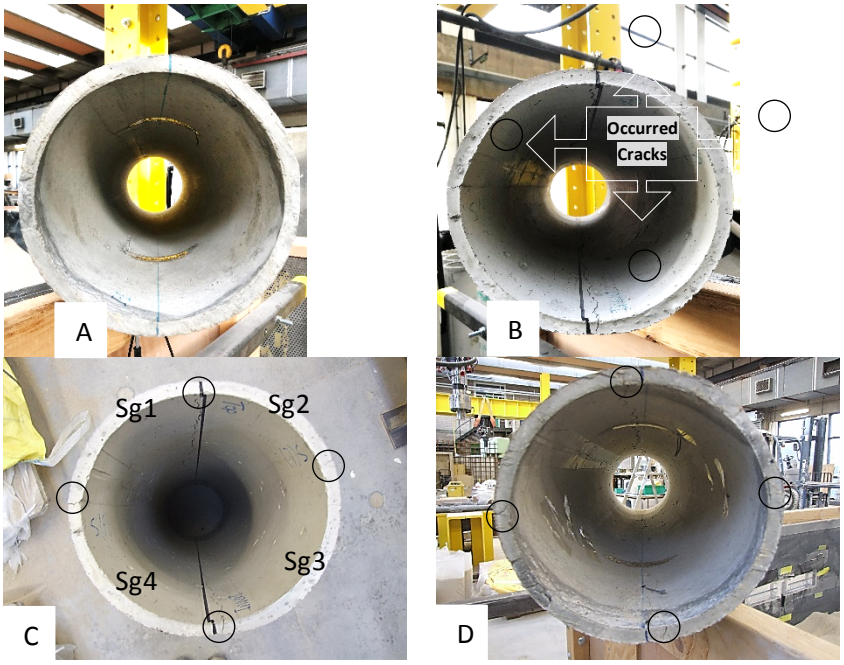

Fig. 10 Deformed cross-section of the pipe, Series B

A: Original. B: N=0. C: N=1. D: N=2. (Sg: segment)

N refers to the number of the geogrid-layers

1268

1269

1270

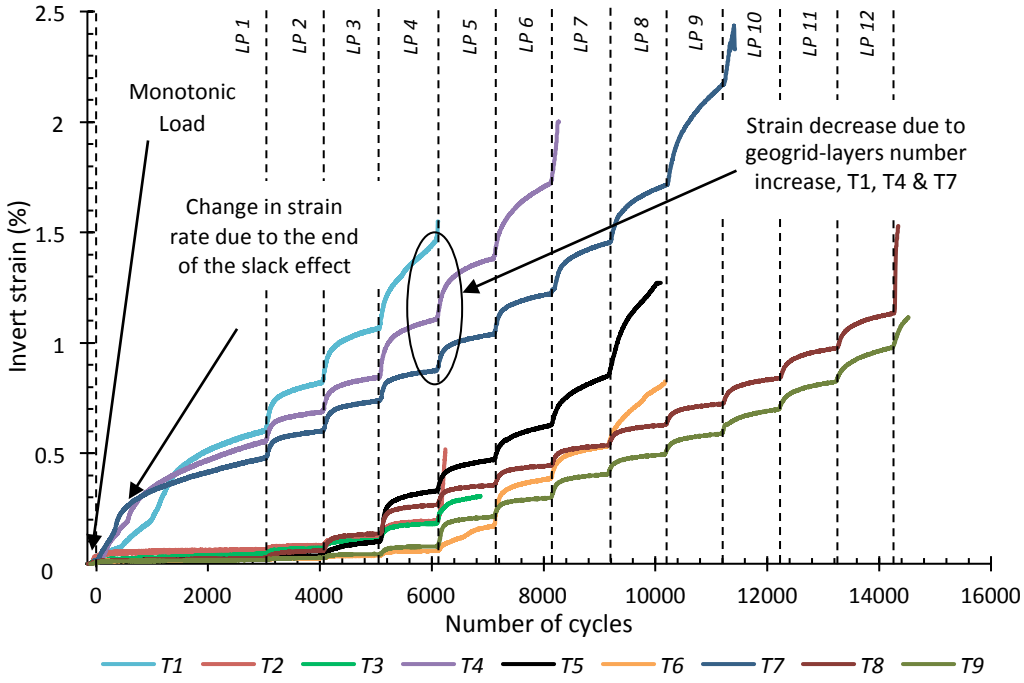

Fig. 11 Invert strain against number of cycles

1271

1272

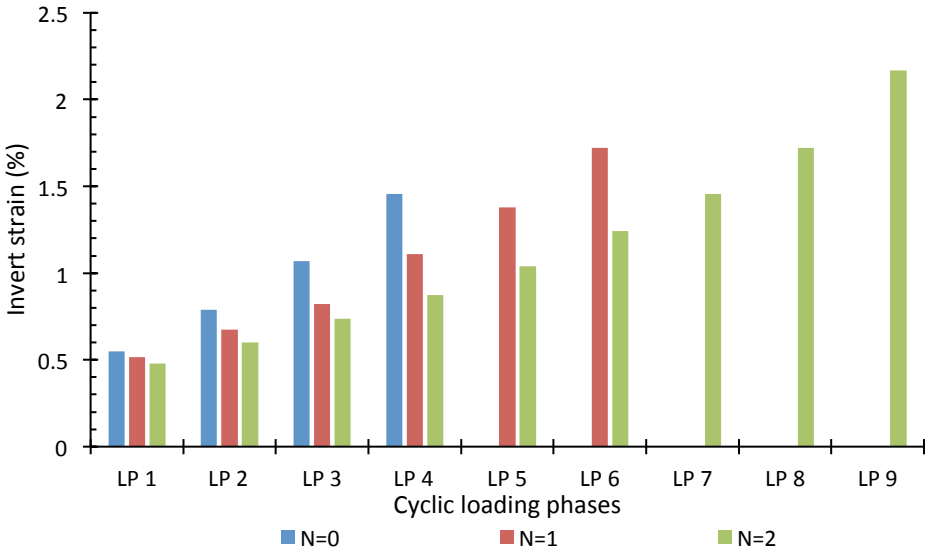

Fig. 12 Influence of geogrid-layers number on strain generated along the invert of the pipe, H/D=1.5

1273

1274

1275

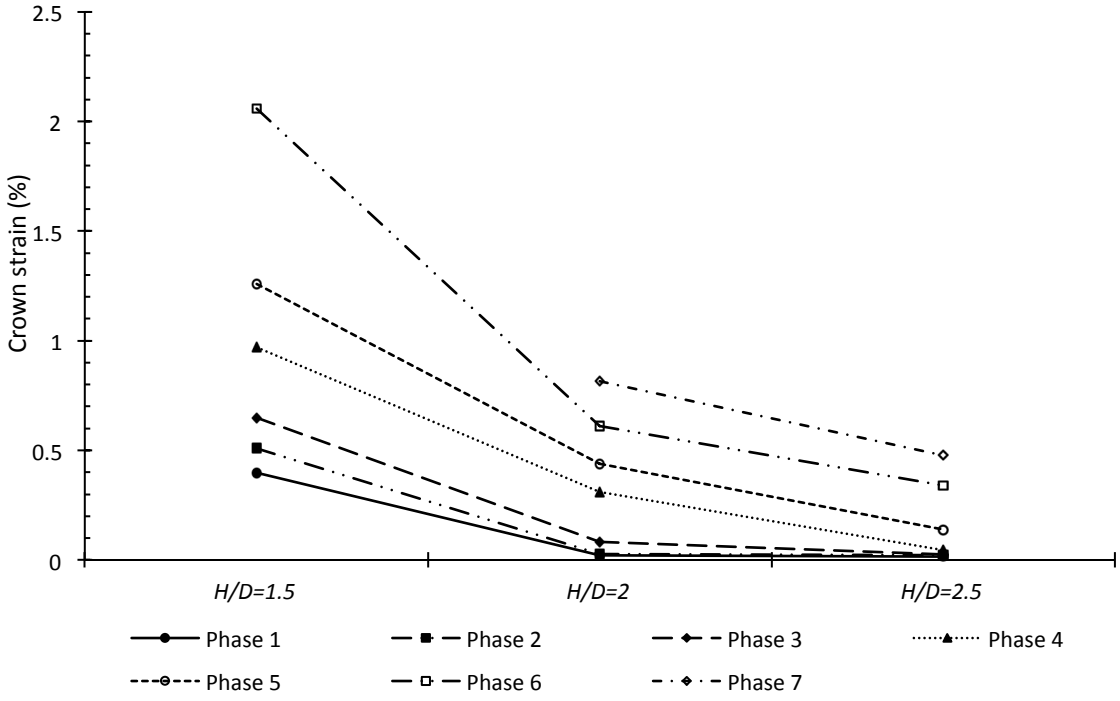

Fig. 13 Crown strain at the end of each loading phase, Series B

1276

1277

1278

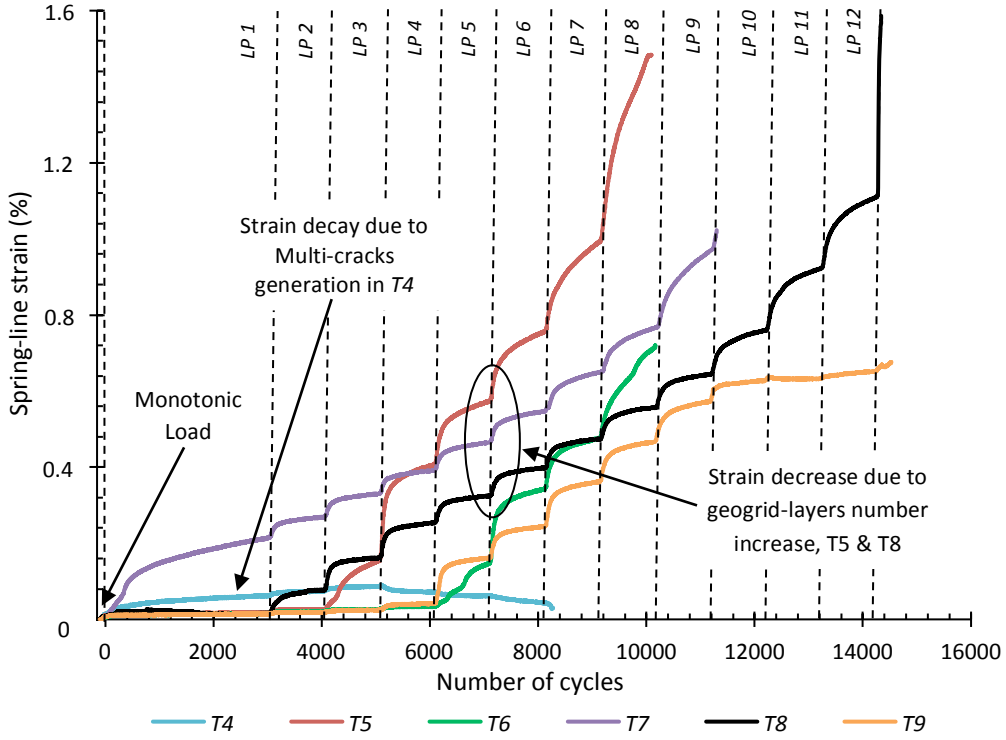

Fig. 14 Spring-line strain due to the progression of loading phases, Series B and C

1279

1280

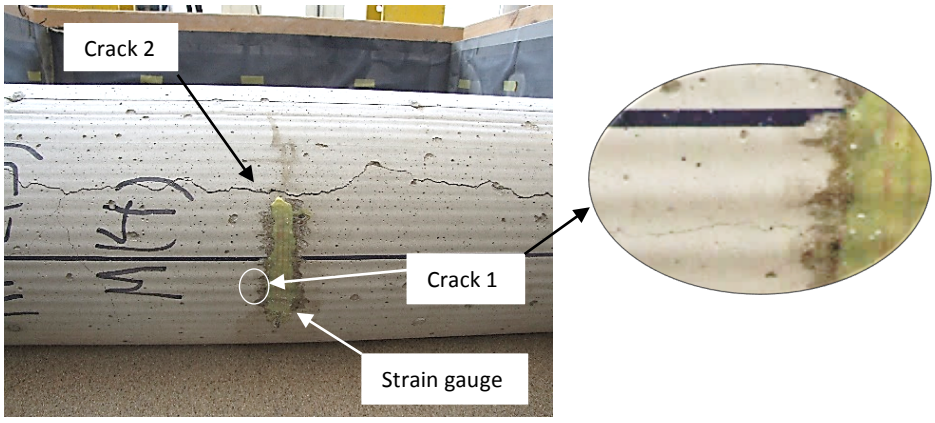

Fig. 15 Cracks along the pipe spring-line in T4

1281

1282

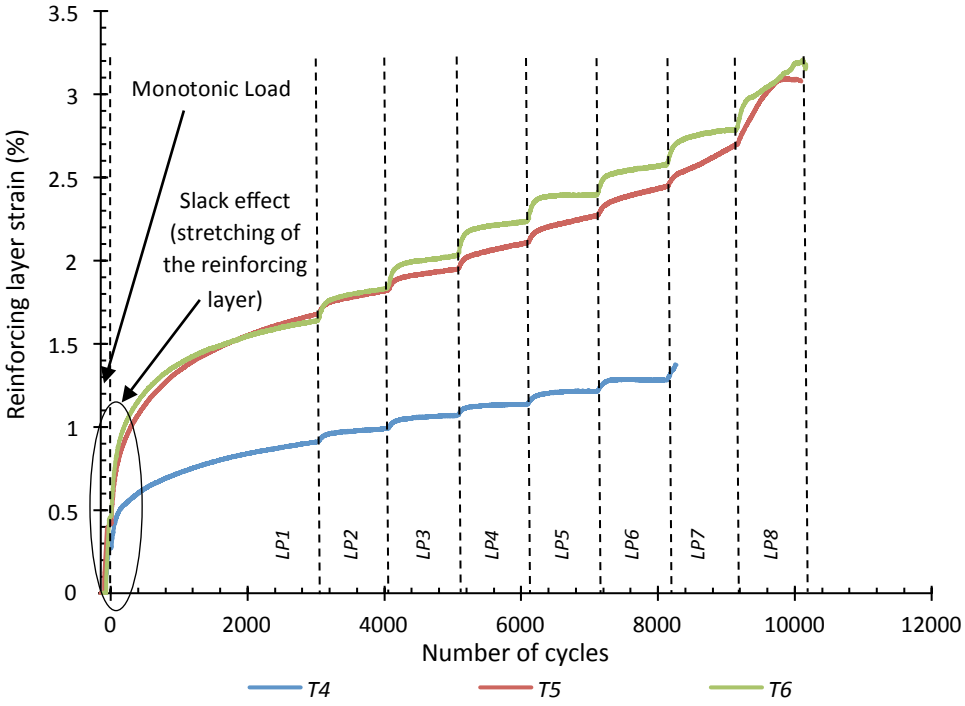

Fig. 16 Strain in the reinforcing layer, Series B

1283

1284

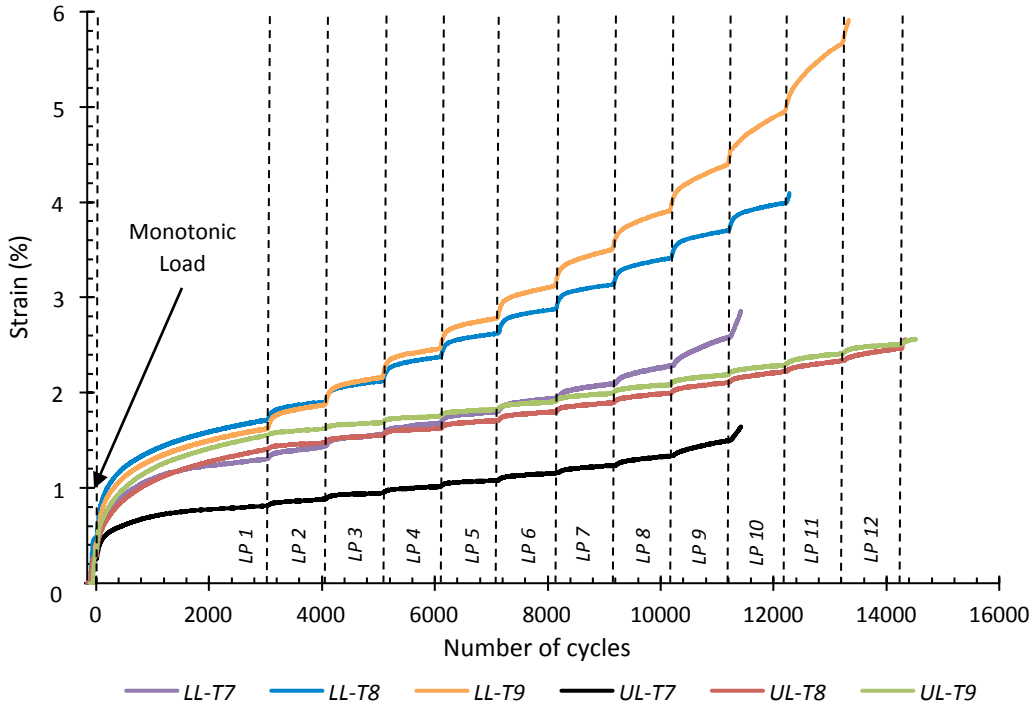

Fig. 17 Strain in the reinforcing layer, Series C

1285

1286

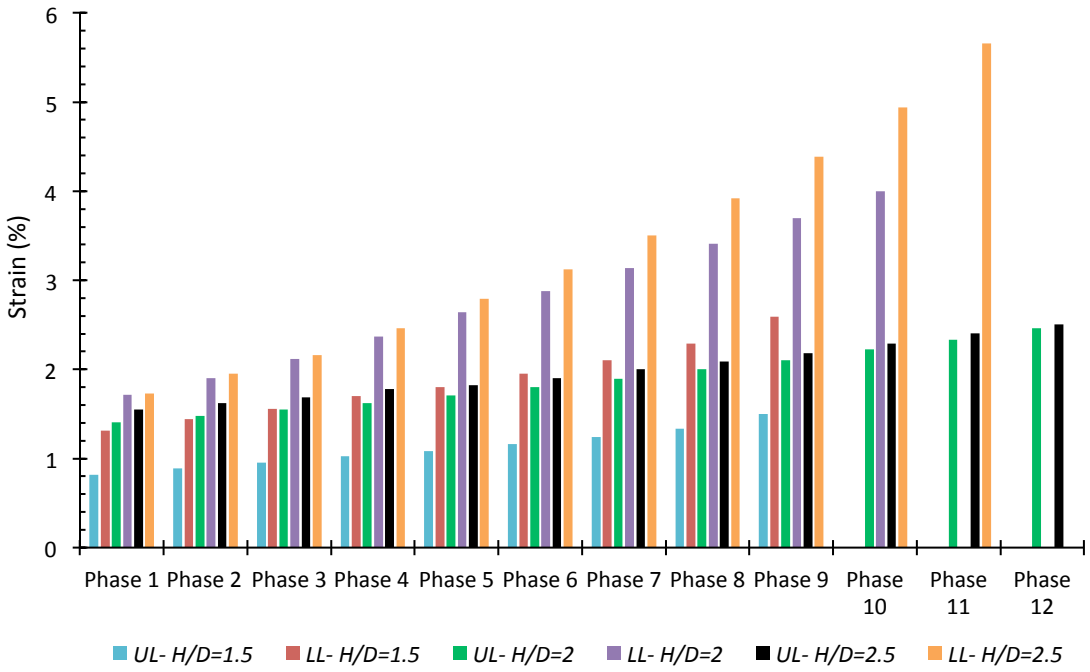

Fig. 18 Comparison between strain in upper and lower layers

1287

1288